JACS
JOURNAL OF THE AMERICAN CHEMICAL SOCIETY
Article
pubs.acs.org/JACS

Quantum Dots as Simultaneous Acceptors and Donors in Time-Gated Förster Resonance Energy Transfer Relays: Characterization and Biosensing

W. Russ Algar,[†,§] David Wegner,[∥] Alan L. Huston,[‡] Juan B. Blanco-Canosa,[⊥] Michael H. Stewart,[‡] Anika Armstrong,[‡,#] Philip E. Dawson,[⊥] Niko Hildebrandt,[∥] and Igor L. Medintz*[,†]

[†]Center for Bio/Molecular Science and Engineering, Code 6900, [‡]Optical Sciences Division, Code 5611, U.S. Naval Research Laboratory, Washington DC 20375, United States

[§]College of Science, George Mason University, Fairfax, Virginia 22030, United States

[∥]Institut d'Electronique Fondamentale, Université Paris-Sud, 91405 Orsay Cedex, France

[⊥]Departments of Chemistry and Cell Biology, The Scripps Research Institute La Jolla, California 92037, United States

[#]Sotera Defense Solutions, Crofton, Maryland 21114, United States

Supporting Information

ABSTRACT: The unique photophysical properties of semiconductor quantum dot (QD) bioconjugates offer many advantages for active sensing, imaging, and optical diagnostics. In particular, QDs have been widely adopted as either donors or acceptors in Förster resonance energy transfer (FRET)-based assays and biosensors. Here, we expand their utility by demonstrating that QDs can function in a simultaneous role as acceptors and donors within time-gated FRET relays. To achieve this configuration, the QD was used as a central nanoplatform and coassembled with peptides or oligonucleotides that were labeled with either a long lifetime luminescent terbium(III) complex (Tb) or a fluorescent dye, Alexa Fluor 647 (A647). Within the FRET relay, the QD served as a critical intermediary where (1) an excited-state Tb donor transferred energy to the ground-state QD following a suitable microsecond delay and (2) the QD subsequently transferred that energy to an A647 acceptor. A detailed photophysical analysis was undertaken for each step of the FRET relay. The assembly of increasing ratios of Tb/QD was found to linearly increase the magnitude of the FRET-sensitized time-gated QD photoluminescence intensity. Importantly, the Tb was found to sensitize the subsequent QD−A647 donor−acceptor FRET pair without significantly affecting the intrinsic energy transfer efficiency within the second step in the relay. The utility of incorporating QDs into this type of time-gated energy transfer configuration was demonstrated in prototypical bioassays for monitoring protease activity and nucleic acid hybridization; the latter included a dual target format where each orthogonal FRET step transduced a separate binding event. Potential benefits of this time-gated FRET approach include: eliminating background fluorescence, accessing two approximately independent FRET mechanisms in a single QD-bioconjugate, and multiplexed biosensing based on spectrotemporal resolution of QD-FRET without requiring multiple colors of QD.

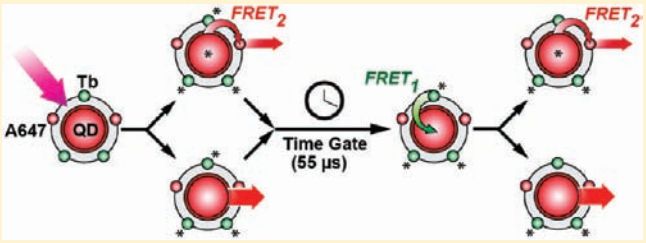

INTRODUCTION

Interest in exploiting the unique properties of colloidal semiconductor quantum dots (QDs) within biological formats continues to grow nearly unabated.[1−4] Pertinent QD properties include broad and strong absorption; bright, narrow, and size-tunable photoluminescence (PL); high quantum yields (QY); resistance to photobleaching; and large two-photon absorption cross sections. Additionally, multiple biomolecular probes can be conjugated to QDs to provide higher avidity and better sensitivity.[1−3] The availability of all these properties in a single entity has made QDs exceptionally useful in energy transfer. In particular, QD-based Förster resonance energy transfer (FRET) configurations are being developed for a variety of applications, including diagnostic assays, target-specific *in vitro* and *in vivo* biosensors, light harvesting, and active nanodevices.[1,5,6]

To date, QDs have most often been used as FRET donors, where their PL properties permit tuning and optimization of the spectral overlap integral, minimization of direct acceptor excitation, reduced crosstalk between QD and dye PL, assembly of concentric multiacceptor architectures to controllably increase FRET efficiency, and facilitated multiplexed FRET configurations.[5,7] A plethora of biosensors relying on QD donors in FRET have been developed for detecting molecular targets that range from ions, nutrients, drugs, and nucleic acids,

Received: November 18, 2011
Published: January 5, 2012

   dx.doi.org/10.1021/ja210162f | J. Am. Chem.Soc. 2012, 134, 1876−1891

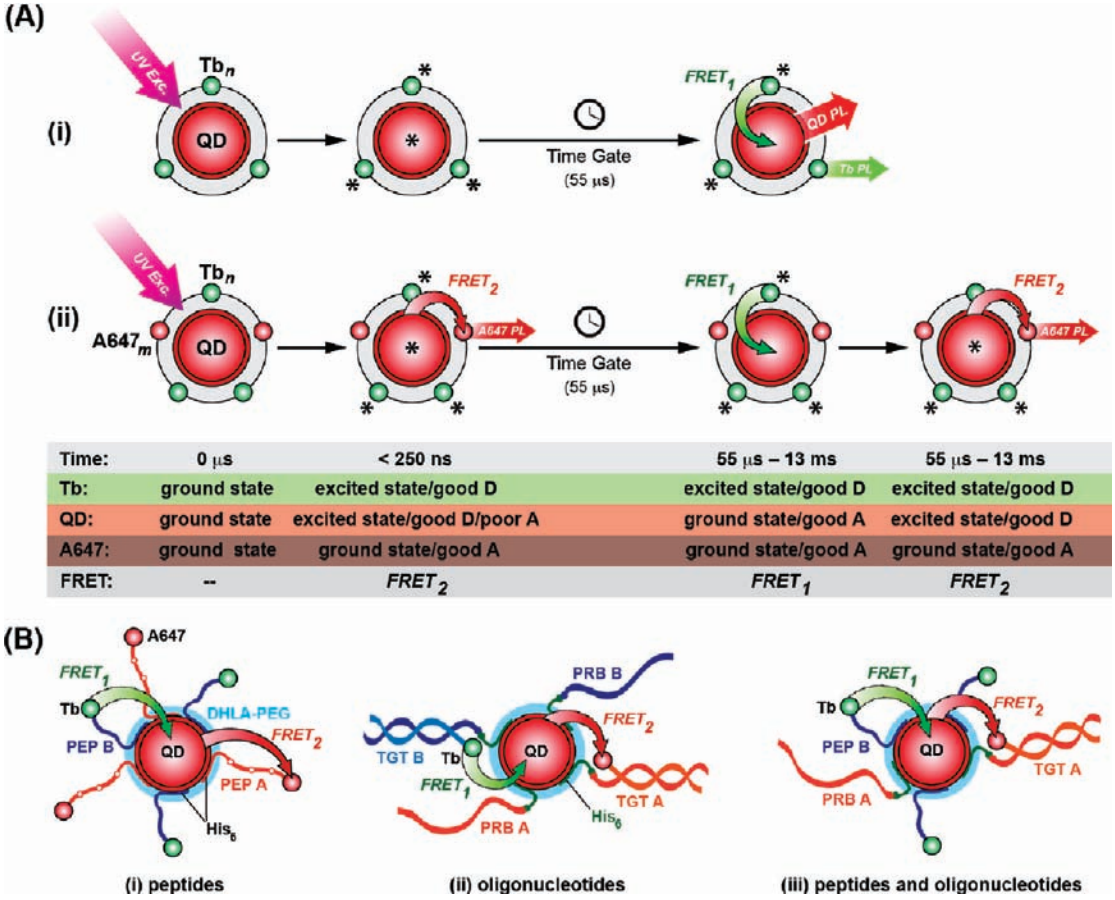

Figure 1. (A) (i) Time-gated FRET sensitization of QD PL via FRET$_1$. Both the Tb and QD are initially excited by a flash of UV light; however, the QD relaxes to its ground state after a suitable microsecond delay (time gate) and becomes a good FRET acceptor for a proximal long-lifetime Tb donor. (ii) Time-gated sensitization of A647 PL via FRET$_1$ and FRET$_2$. The coassembly of a fluorescent dye, A647, with the Tb around a QD permits a two-step energy transfer relay with the QD as an intermediary. (B) The QD is able to serve as a nanoscaffold for the controlled assembly of biomolecules labeled with Tb and A647. Three configurations are used in this work: (i) peptide assembly, (ii) oligonucleotide assembly and hybridization, and (iii) both peptide and oligonucleotide assembly/hybridization.

to enzymatic processes such as proteolysis and phosphorylation (see refs 2, 3, 5, and 7 for reviews). In contrast, the role of QDs as FRET acceptors is more complicated and much less utilized. The principle challenge is that putative QD acceptors are more efficiently excited than most potential donors—for example, molecular dyes—as a result of their broad absorption and their larger (~10- to 100-fold) extinction coefficients. QDs also have longer excited-state lifetimes (≥10 ns) than most fluorescent dye donors (≤5 ns). These combined attributes can preclude viable energy transfer using optical excitation and QD acceptors;[8] however, this limitation has been overcome in practice using three elegant solutions. First, Hildebrandt et al. showed that QDs were good FRET acceptors for luminescent lanthanide ion donors that had millisecond excited-state lifetimes, thereby allowing the QD excited-state to decay prior to energy transfer.[9] Lanthanide–QD FRET pairs offer very large spectral overlap integrals and Förster radii (R_0 ~ 10–11 nm),[9,10] as well as excellent capacity for multiplexing.[11,12] Second, Rao's group used QDs as an acceptor for bioluminescent luciferase donors, thereby avoiding optical excitation and preserving the QD as a ground state acceptor.[13,14] Four-color *in vivo* imaging and a two-color protease assay were demonstrated using this approach.[13,14] Third, Willner's group has demonstrated the use of QD acceptors in multiplexed sensing configurations using chemiluminescent donors.[15,16] Note that the use of QD donor–QD acceptor FRET pairs is possible given the more compatible excited-state lifetimes[17−19] but is nonideal because of the large amount of direct QD acceptor excitation and the challenge of physically assembling well-defined QD-QD FRET pairs.

Beyond single-step donor–acceptor configurations, interest in incorporating QDs within multistep, biomolecularly assembled FRET relays has grown. QD–dye–dye configurations have been used to extend the distance range of FRET via an energy relay at the intermediate fluorophore.[20−22] More recently, QDs were shown to function as potent initial donors for a four-step FRET cascade along the length of DNA wires decorated with a series of fluorescent dye acceptors.[23] The use of a QD as an optimal initial donor is common to these studies; however, subsequent energy transfer step(s) have remained limited by the properties of dyes. Given the advantages of using QDs as either an acceptor or a donor, it follows that a QD is best suited as an intermediary in a FRET relay where it can simultaneously function in both roles and enhance both energy transfer steps. The approximate centrosymmetry and surface area of the QD are also ideal for the coassembly of multiple initial donors and/or final acceptors to optimize energy transfer rates. However, the role of QDs as an intermediary in FRET relays remains largely unexplored and underutilized.

dx.doi.org/10.1021/ja210162f | *J. Am. Chem.Soc.* 2012, 134, 1876–1891

In this work, we assemble and characterize biomolecular assemblies of Tb^{3+} complex (Tb)-to-QD-to-Alexa Fluor 647 (A647) fluorescent dye multistep FRET relays with strong potential for biosensing. The concept and assemblies are illustrated in Figure 1. We first characterize the photophysical properties of the relay, including the progressive time-gated Tb-sensitization of the QDs via FRET step 1 ($FRET_1$) and subsequent QD-to-A647 energy transfer via FRET step 2 ($FRET_2$). Time-gating is essential to the observation of $FRET_1$ and the subsequent energy relay via $FRET_2$. Next, we apply the time-gated FRET relay to prototypical protease and nucleic acid biosensing assays. We then demonstrate that the new temporal dimension of information provided by the FRET relay permits resolution of the two different energy transfer pathways when coupled to biomolecular binding events, thereby potentiating multiplexed, spectrotemporal detection using a single QD-bioconjugate. These applications clearly show the QDs to be an ideal nanoscale platform and intermediary for FRET relays.

MATERIALS AND METHODS

Reagents. CdSe/ZnS QDs were provided by Invitrogen by Life Technologies (Carlsbad, CA) and functionalized with dihydrolipoic acid-appended poly(ethylene glycol) (PEG, MW~750) ligands in-house.[24,25] Peptides were synthesized as described[26,27] and labeled using A647 maleimide (Invitrogen) or Lumi4 Tb^{3+} *N*-hydroxysuccinimide (NHS) complex (Tb; Lumiphore, Richmond, CA).[28] Probe and complementary target oligonucleotides were obtained from Integrated DNA Technologies (Coralville, IA). Targets were labeled with A647 or Tb; probes were modified to hexahistidine (His_6)–DNA–peptide chimeras.[27] Peptide and oligonucleotide sequences are given in Table 1, and the labeling chemistry is shown in Scheme 1.

Table 1. Peptide and Oligonucleotide Sequences[a]

peptides (written N- to C-terminal):	
PEP A[b]	(A647)–CSTRIDEANQRATKLP$_7$SH$_6$
PEP B[c]	(Lumi4 Tb^{3+})–GSGAAAGLSH$_6$
oligonucleotides (PRB = probe, TGT = target):	
PRB A[d]	3′- *tta gtt ctg tta taa caa*–5′–CGSGAAAGLSH$_6$
TGT A	5′–*aat caa gac aat att gtt*–3′–(A647)
PRB B[d]	3′- *caa cat cct aat tga ctt*–5′–CGSGAAAGLSH$_6$
TGT B[c]	5′–*gtt gta gga tta act gaa*–3′–(Lumi4 Tb^{3+})

[a]Amino acid residues are capitalized in normal font; nucleotides are given in lower case italics. [b]Peptide labeled at the cysteine (thiol). [c]Peptide labeled at the N-terminus (1° amine), oligonucleotide labeled at a 3′-amino linker. [d]Peptide–oligonucleotide chimeras are linked by a disulfide bridge between the peptide cysteine residue and 5′-thiol linker on the oligonucleotide.

Instrumentation and PL Measurements. PL spectra were acquired using a Tecan Infinite M1000 dual monochromator multifunction plate reader equipped with a xenon flash lamp (Tecan, Research Triangle Park, NC). Nongated PL emission spectra: 400 Hz flash frequency, 400 nm excitation, ~0 μs delay between flash and data acquisition, and a 40 μs integration time. Time-gated PL emission spectra: 100 Hz flash frequency, 339 nm excitation, 55 μs delay, 1 ms integration time. Tb/QD PL decay time measurements were acquired using three different systems (PLD systems 1–3), each with optimized capabilities for different decay time scales (see the Supporting Information).

QD Bioconjugates and Assays. A647/Tb labeled peptides/oligonucleotides were conjugated to QDs via polyhistidine self-assembly by mixing at the desired stoichiometric ratios, in buffer, for 30–60 min. No purification was necessary, and the well characterized, high-affinity binding resulted in nearly quantitative assembly to the QDs.[22,29–31] Because the labeled peptides were quantitated using the Tb/A647 absorption, this ensured knowledge of the number of donors/acceptors per QD. For characterization experiments, the QD conjugate concentration was 45 nM (5 pmol). Time-gated proteolytic assays were done by preparing $(PEP\ B–Tb)_{10}$–QD–$(PEP\ A–A647)_3$ conjugates, adding trypsin, and tracking time-gated PL at 625 and 675 nm over 1.5 h at 2 min intervals. The final QD conjugate concentration was 0.2 μM (20 pmol). Time-gated hybridization assays were done by mixing TGT A–A647 (0–50 pmol) with 60 pmol of PRB A, hybridized 60 min, $(PEP\ B–Tb)_{10}$–QD conjugates added, and time-gated PL spectrum measured after 60 min. The final QD conjugate concentration was 45 nM (5 pmol). Two-plex hybridization assays were done similarly, except that TGT A (0–50 pmol) and TGT B (0–80 pmol) were mixed with 50 pmol of PRB A and 80 pmol of PRB B prior to the addition of unconjugated QDs. Both nongated and time-gated PL spectra were measured.

A full description of all reagents, experimental methods, instrumentation, and analysis is provided in the Supporting Information.

RESULTS

Self-Assembly of QD-Peptide and DNA Bioconjugates. Control over the number of A647 and Tb assembled to a central QD was critical to the experimental results presented here. Therefore, the peptides and peptide–oligonucleotide chimeras used in this study were engineered to display terminal His_6 metal-affinity sequences to provide spontaneous self-assembly to the Zn^{2+}-rich QD surface.[31] Our group, as well as several others, has frequently used this motif to prepare QD bioconjugates of proteins, peptides, and oligonucleotides with excellent control over the conjugate valence.[22,29,30] Characterization of His_6 self-assembly to QDs confirmed that an average 50 ± 10 peptides can be assembled around a ~6 nm diameter DHLA-capped QD.[32] The 625 nm emitting QDs used in this study were coated with a similar ligand but were ~10 ± 1 nm in diameter (data not shown), suggesting access to an even wider range of conjugate valences. Because our experiments required the assembly of peptides and oligonucleotides, the latter were chemically ligated with a His_6-appended peptide[29] (Scheme 1, Table 1) to ensure a level of control that was analogous to peptide assembly. In turn, labeling the peptides or oligonucleotides with Tb and/or A647 (Scheme 1) enabled excellent control over the number of Tb and A647 assembled per QD; this permitted characterization of the $FRET_1$ and $FRET_2$ processes (depicted in Figure 1A) during stepwise changes in donor–acceptor stoichiometry. The schematic constructs in Figure 1B summarize the three different QD bioconjugates used here: (i) peptides, (ii) peptide–oligonucleotide chimeras, and (iii) hybrid assemblies of peptides and peptide–oligonucleotide chimeras. Because the assembly of these labeled materials to the QD yields an approximately centrosymmetric FRET configuration, it was possible to treat all of the Tb or A647 in a given assembly as being equivalent within the Förster formalism (see the Supporting Information).

Donor–Acceptor Pairs and Spectral Overlap. Red-emitting 625 nm PL QDs (27 nm full width at half-maximum (FWHM)) were paired as both an acceptor for the initial Tb donor and a subsequent donor for the A647 acceptor. Figure 2 shows the absorption and PL spectra for the Tb, QD, and A647, as well as the spectral overlap functions for the Tb–QD and QD–A647 FRET pairs. Photophysical and FRET parameters for the different luminophores and donor–acceptor combinations are listed in Table 2. The Tb^{3+} complex

Scheme 1. Bioconjugate Chemistries

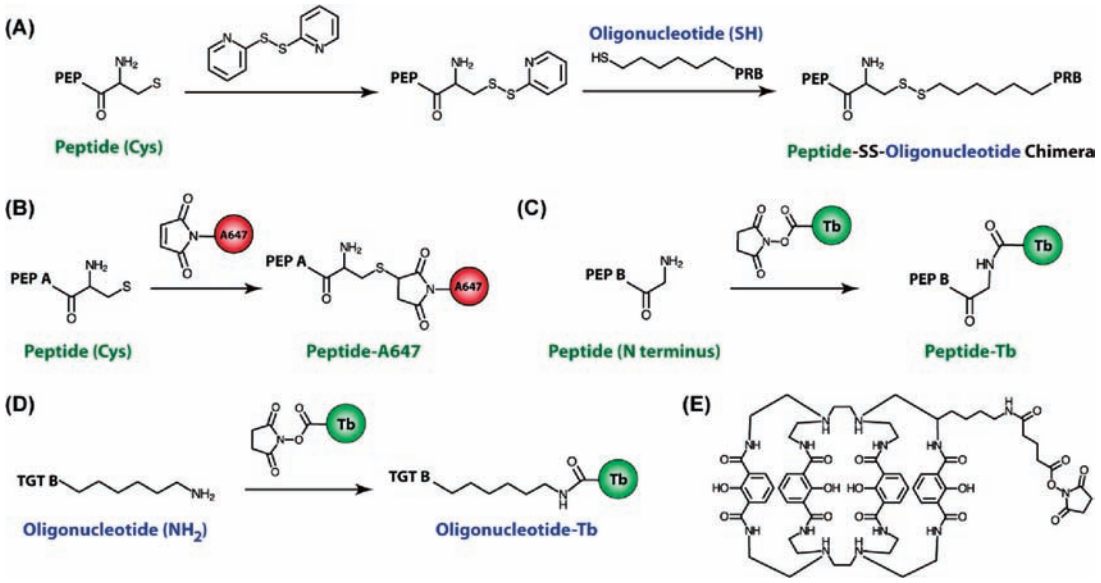

(A) Pyridyl disulfide activation of thiolated-peptide and a disulfide exchange reaction to prepare His_6–peptide–oligonucleotide chimeras. (B) A647-maleimide PEP A labeling at an N-terminal cysteine residue. (C) Tb-NHS PEB B labeling at the N-terminus. (D) Tb-NHS labeling at an amino modified linker of TGT B. Actual linker structures shown for the oligonucleotide amine and thiol reactions. (E) Lumi4 NHS ligand structure (Tb^{3+} omitted for clarity).

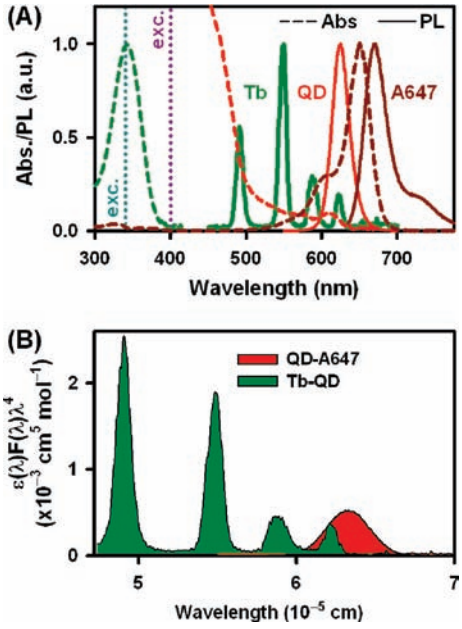

Figure 2. (A) Absorbance and PL spectra for the Lumi4 Tb^{3+} complex (as PEP B–Tb), red-emitting CdSe/ZnS QDs, and A647 dye (as PEP A–A647); 339 and 400 nm excitation are shown for reference. (B) Spectral overlap functions for the Tb–QD and QD–A647 FRET pairs.

incorporates a proprietary isophthalamide-type ligand that sensitizes the lanthanide ion, which otherwise has a prohibitively low direct molar absorptivity.[28,33] The Tb was optimally excited at 339 nm and exhibited sharp emission lines at ~ 490, 550, 585, and 620 nm. The QD was also efficiently excited at 339 nm ($\varepsilon_{QD} \approx 1.9 \times 10^7$ M^{-1} cm^{-1}) and 400 nm ($\varepsilon_{QD} \approx 1.1 \times 10^7$ M^{-1} cm^{-1}). In contrast, the A647 was only very weakly excited at these wavelengths ($\varepsilon_{A647} \leq 1 \times 10^4$ M^{-1} cm^{-1}).

The remarkably large Förster distance calculated for Tb-to-QD energy transfer (10.1 nm) was a product of the extremely strong absorption of the QD across the emission range of the first three Tb lines. The Förster distance of the QD–A647 FRET pair was 7.5 nm, and this value is among the largest noted when pairing a QD donor with a dye acceptor (typically, R_0 < 6 nm). Examining the Tb–QD–A647 three-luminophore system *a priori* confirmed the potential for a multistep $FRET_1$ + $FRET_2$ relay process, wherein excited-state Tb can transfer energy to the QD (acceptor), which subsequently acts as a donor for the A647, resulting in a net energy transfer from the Tb to the A647. We also note that the putative Tb–A647 FRET pair had significant spectral overlap and a Förster distance of 5.7 nm ($J = 2.5 \times 10^{-10}$ mol^{-1} cm^6); however, the $FRET_1$ and $FRET_2$ pathways should be more favored because, based on the relative Förster distances, their rates are expected to be 30-fold and 5-fold faster than Tb-to-A647 energy transfer, respectively (see the Supporting Information).

Intensity-Based Analysis of Tb-to-QD Energy Transfer ($FRET_1$). Initial experiments focused on determining the degree to which the Tb could sensitize time-gated QD PL via $FRET_1$. Increasing ratios of Tb-labeled PEP B (PEP B–Tb) were assembled on the 625 nm QDs, and the resulting PL spectra were collected in both nongated (~0 μs delay) and time-gated modes (see the Materials and Methods section for exact definitions). Time-gating for the measurements was empirically selected to be 55 μs, which corresponded to the minimum delay after flash excitation needed to minimize signal from direct excitation of the QDs. The residual signal was due to an instrumental/electronic echo effect rather than residual PL, as the QD excited-state completely decayed in less than a microsecond. An integration time of 1 ms was selected for time-gated measurements to be commensurate with the typical excited-state lifetimes of Tb complexes.[33] Without time-gating, the Tb sensitization of QD PL could not be observed over the directly excited QD PL (Figures S4 and S5 in the Supporting

dx.doi.org/10.1021/ja210162f | J. Am. Chem.Soc. 2012, 134, 1876–1891

Table 2. Optical Characteristics of Tb, QD, and A647 Luminophores with Their FRET Pairs

luminophore	ε_{max} (M^{-1} cm^{-1}) [λ_{max}]	ε (M^{-1} cm^{-1}) [λ_D][a]	Φ	τ
Tb	26 000 [339 nm] (Lumi4 ligand)		0.77 ± 0.10 (Tb^{3+})	2.6 ± 0.2 ms
QD	5.5×10^5 [610[b] nm]	$5-50 \times 10^5$ [475–575 nm]	0.55 ± 10	50 ± 3 ns
A647	239 000 [650 nm]	89 000 [625 nm]	0.33[c]	~1 ns[d]

FRET pair (D → A)[e]	J (mol^{-1} cm^6)	R_0 (nm)
Tb → QD	7.2×10^{-9}	10.1
QD → A647	1.8×10^{-9}	7.5

FRET pairs (D → A)[e]	$r_{pred.}$ (nm)[f]	$r_{meas.}$ (nm)	FRET modality
PEPB–Tb → QD[g]	6.2 – 6.7	6.3	$FRET_1$ (Tb lifetime quenching)
QD → PEPA–A647[h]	7.7 – 8.2	8.4	$FRET_2$ (QD PL quenching)
QD → PEPA–A647[i] nongated with $(PEPB–Tb)_{10}$	7.7 – 8.2	8.3	$FRET_2$ (QD PL quenching)
QD → PEPA–A647[j] time-gated with $(PEPB–Tb)_{10}$	7.7 – 8.2	8.1	$FRET_2$ (QD PL quenching)

[a]Extinction coefficient at peak donor PL emission wavelength, λ_D. [b]Extinction coefficient at first exciton peak. [c]Source: Invitrogen by Life Technologies. [d]Source: ref 55 [e]Written as donor to acceptor. [f]Geometric prediction based on QD and peptide dimensions. [g]Tb → QD measured from Tb PL decay quenching. [h]QD → A647 measured from QD PL quenching following direct QD excitation. [i]QD → A647 measured from nongated QD PL quenching following direct QD excitation (PEP B–Tb also present on QD). [j]QD → A647 measured from time-gated QD PL quenching following $FRET_1$ sensitization.

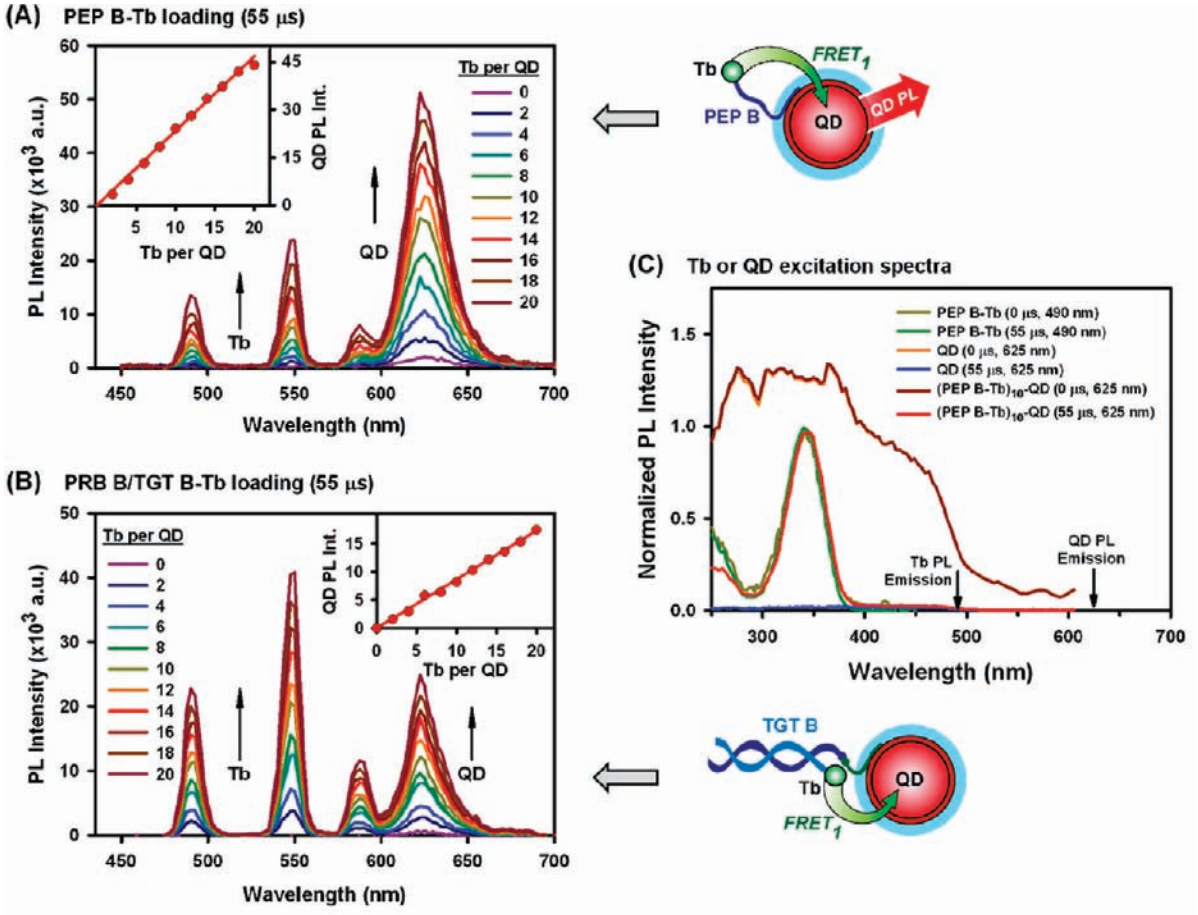

Figure 3. Time-gated (55 μs) PL spectra showing the increasing $FRET_1$-sensitization of QD PL with an increasing amount of (A) PEP B–Tb and (B) PRB B/TGT B–Tb hybrids (the valence of PRB B is consistently 20). In each case, the insets show an approximately linear increase in $FRET_1$-sensitized QD PL. (C) Nongated (~0 μs) and time-gated (55 μs) PL excitation spectra for QD, PEP B–Tb, and conjugates collected at Tb (490 nm) and QD (625 nm) PL emission wavelengths.

Information compare the absolute PL intensities for each individual luminophore component and QD conjugate at equivalent detection settings).

As shown in Figure 3A, an approximately linear increase in the time-gated, Tb-sensitized QD PL was observed as the valence of PEP B–Tb assembled per QD was incrementally increased from 0 to 20 Tb per QD. An analogous experiment using the same ratios of prehybridized Tb-labeled TGT B/PRB B peptide–DNA chimeras (PRB B/TGT B–Tb) is shown in Figure 3B and also revealed an approximately linear increase in

dx.doi.org/10.1021/ja210162f | J. Am. Chem.Soc. 2012, 134, 1876–1891

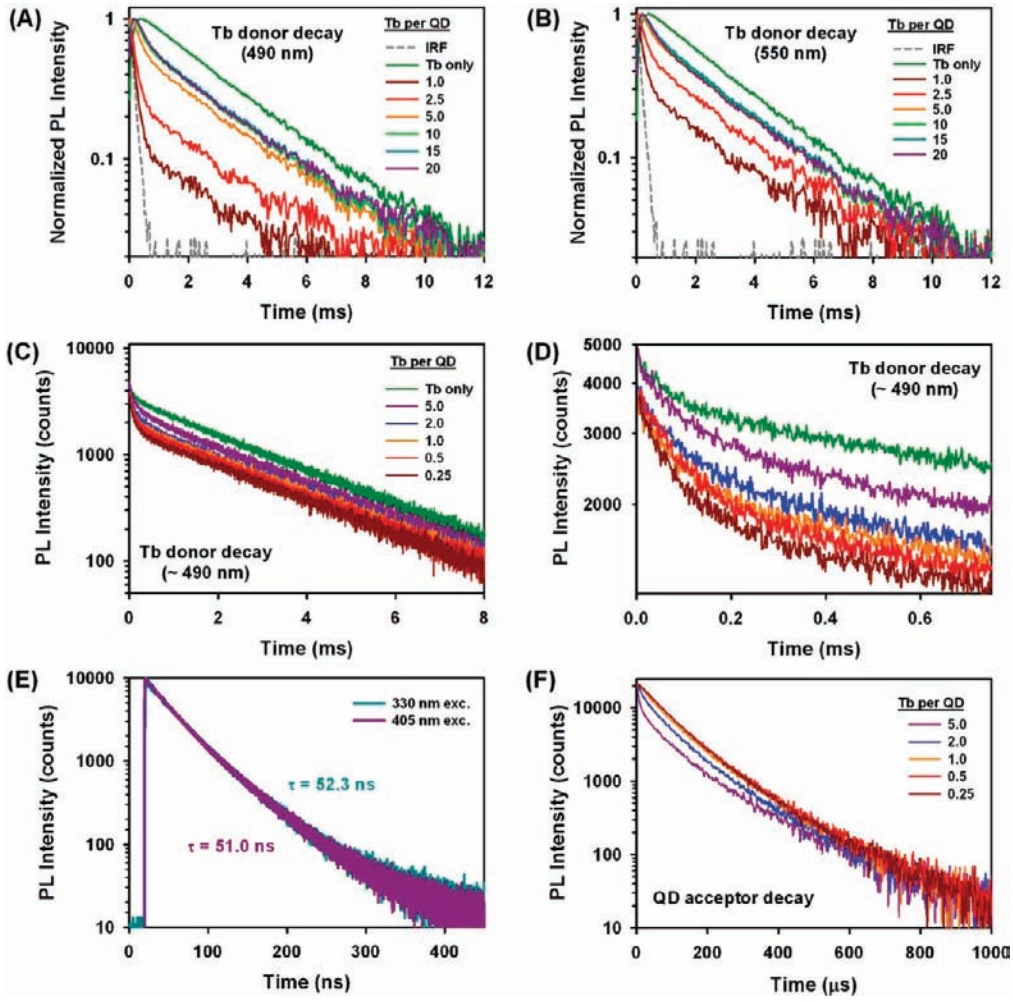

Figure 4. Tb donor PL decay curves collected at (A) 490 nm and (B) 550 nm for different PEP B−Tb/QD ratios using PLD system 1. (C) Higher-resolution donor PL decay curves collected at 490 nm for the indicated PEP B−Tb/QD ratios using PLD system 2. (D) Magnified view of the short PL lifetime component for the data in part C. The small fraction of short PL lifetime component in the green (Tb only) curve is an artifact from the detection setup. (E) Native QD PL decay curves. (F) $FRET_1$-sensitized QD PL decay curves at different PEP B−Tb/QD ratios. The QD reflects the ca. 10^2 μs lifetime associated with energy transfer from the Tb.

QD sensitization. Increased time-gated QD sensitization was also observed beyond 20 Tb per QD, but the linear trend was not always consistent. Moreover, these higher valences were not pursued because we sought to avoid potential nearest-neighbor effects. In the case of the PRB B/TGT B−Tb loading, nonspecific adsorption of TGT to the QDs was found to be negligible (see Figure S7 in the Supporting Information). Clearly, the long excited-state lifetime of the Tb provided sufficient time for the QD to relax to its ground state (following flash excitation) and function as an effective FRET acceptor. In turn, the time-gating provided a mechanism to monitor this process. It is also critical to note that the time-gated QD PL signal was minimal in the absence of assembled Tb, confirming that the His_6-mediated selective attachment of the Tb-labeled peptides/oligonucleotides to the QD and thereby sensitized the time-gated QD PL.

Importantly, the Tb functioned as an effective FRET donor for the QD irrespective of whether it was directly labeled onto a peptide terminus (PEP B−Tb) or indirectly through oligonucleotide hybridization (PRB B/TGT B−Tb). We attribute the slightly lower rate of QD sensitization or FRET efficiency for the latter to a slightly longer Tb−QD separation in the DNA incorporating configuration. The Tb was attached at the end of a six-carbon aminated linker, which can allow some freedom of movement, in addition to breathing of the oligonucleotide hybrids. Moreover, previous results suggest that dye labels assembled onto QDs using similar peptide−DNA chimeras can have a wide range of movement relative to the QD.[34] Regardless, assembling greater numbers of Tb around the central QD increased the rate of energy transfer from Tb donors to QD acceptors, and this effect was observed as increases in the time-gated QD PL sensitization.

To further assess $FRET_1$, the excitation spectra of $(PEP\ B{-}Tb)_{10}$−QD conjugates were measured with and without time-gating, as shown in Figure 3C. In both cases, the Tb emission (monitored at 490 nm), gave rise to the characteristic PEP B−Tb excitation/absorption peak centered at 339 nm. In contrast, monitoring the QD PL (at 625 nm) produced three very different results. The characteristically broad QD excitation/absorption spectrum was observed without time-gating for QD alone or $(PEP\ B{-}Tb)_{10}$−QD conjugates. With time-gating, the QD alone yielded no signal, whereas $(PEP\ B{-}Tb)_{10}$−QD conjugates exhibited the characteristic Tb excitation/absorption peak centered at 339 nm. The latter indicated that energy

dx.doi.org/10.1021/ja210162f | J. Am. Chem.Soc. 2012, 134, 1876−1891

absorbed by the Tb was being re-emitted by the QD. These results provided additional confirmation of QD sensitization by the Tb once the QD had returned to its ground state following direct optical excitation.

Finally, we noted that marked quenching of the Tb donor PL intensity—especially at higher assembly ratios—could not be consistently observed in the time-gated PL spectra. This result did not allow for measurement of FRET efficiency directly from the donor PL loss and is in contrast to previous formats where QD donors were assembled with an increasing number of acceptors, resulting in progressive quenching of the QD PL.[20,35−38] However, given the multiple donor−single acceptor configuration, this behavior was not unexpected, as we later discuss.

PL Decay Analysis of Tb-to-QD Energy Transfer ($FRET_1$). Further characterization and confirmation of Tb-to-QD energy transfer was obtained using PL decay time analyses. Measurements of the Tb PL lifetimes were first collected, using PLD system 1 (see the Supporting Information), as the number of PEP B−Tb assembled per QD was increased. As shown in Figure 4A and B, the Tb lifetimes were monitored at both the 490 and 550 nm emission lines. In the absence of QD, the PEP B−Tb had a monoexponential PL decay with a characteristic lifetime of ca. 2.6−2.7 ms. When an average of ∼1 PEP B−Tb was assembled per QD, the PL decay became distinctly multiexponential, showing a fast decay component and a residual long-lifetime component that paralleled the native Tb lifetime. As the average number of PEP B−Tb was increased to 2.5, 5, 10, 15, and 20 per QD, the relative contribution of the native, long-lifetime component increased significantly; however, the fast decay component did not fully disappear. At >10 PEP B−Tb/QD, the ratio of the fast and native decay components saturated to a constant value. This behavior was reflected in both the 490 and 550 nm Tb PL lines, although, for the 550 nm line, the fast decay appeared more attenuated compared to the native, long-lifetime component of the Tb. This disparity coincided with the relative brightness of the Tb lines (550 nm > 490 nm; see Figure 2A).

The appearance of the very fast decay component was consistent with very efficient energy transfer from the Tb to QD, as expected, based on the large R_0 of 10.1 nm for this FRET pair. We estimated that the PEP B−Tb places the Tb ≤ 1.2 nm from the QD surface and ∼6.7 nm from the QD center. This value was arrived at by considering (1) a negligible contribution from the His_6-terminus, which is in direct contact with the ZnS shell; (2) the Ala_3 tract forming a helix that is disrupted by the flanking glycine residues; (3) rotational flexibility in the peptide; and (4) comparison to donor−acceptor distances for similarly sized peptides determined previously.[38] The QD radius was estimated to be 5.5 nm. As the Tb donor−QD acceptor separation ($r \approx 6.7$ nm) was much shorter than the Förster distance (10.1 nm), a FRET efficiency exceeding 92% was expected (eq S5, Supporting Information). The short Tb lifetime component was between ca. 20−200 μs (see Tables S1 and S2 in the Supporting Information for full fitting and analysis parameters) and suggested $FRET_1$ efficiencies of 93−99% (eq S8, Supporting Information). However, these short lifetimes were comparable to the temporal resolution (40 μs) of PLD system 1 measurements; further experiments were done at higher resolution (2 μs bins) using PLD system 2. Representative data measured for different ratios of Tb/QD (490 nm emission line) are shown in Figure 4C and D and are summarized in Table 3 (see Tables S3 and S4 in the Supporting Information for full fitting and analysis parameters). Only low conjugate valences were used with PLD system 2 because they revealed the most striking changes. The short, QD-quenched, Tb decay component(s) were analyzed in detail and yielded an average lifetime of 150 ± 60 μs, which corresponded to a $FRET_1$ efficiency of approximately 94 ± 3%. Based on this data, we estimated the rate of $FRET_1$ to be 6.3×10^3 s^{-1} (see the Supporting Information).

Table 3. $FRET_1$ Efficiencies Determined from $FRET_1$-Quenched Tb PL Decay Lifetimes and $FRET_1$-Sensitized Time-Gated QD PL Decay Lifetimes (Collected with PLD System 2).[a]

	Tb PL (490 nm)			QD PL	
Tb per QD	$^{Tb\text{-}FRET}\tau_{av}$ (μs)	$\tau_3 = \tau_{Tb}$ (ms)	E_{Tb}[b]	$^{QD\text{-}FRET}\tau_{av}$ (μs)	E_{QD}[c]
0		2.72		0.05[d]	0
0.5	159	2.72	0.95	133	0.95
1	172	2.73	0.95	119	0.96
2	136	2.74	0.94	114	0.96
5	126	2.72	0.94	113	0.96

[a]Refer to Tables S1−S4 in the Supporting Information for full PL decay data sets, including data collected using PLD system 1. [b]$FRET_1$ efficiency from fast Tb PL decay component. [c]$FRET_1$ efficiency from time-gated sensitized QD PL decay. [d]QD in the absence of FRET; measured with PLD system 3 (see the Supporting Information).

Because of the electronic saturation of PLD system 2 at short time-scales, some residual fast decay component appeared in the PEP B−Tb decay curves (see Figure 4D). This was a result of the high sensitivity of PLD system 2 and its optimization for long-lifetime measurements. Although this contribution was very small, it was important to compare the lifetime results from the Tb donor decays with the Tb-sensitized QD PL decays. The latter are proof of FRET because microsecond to millisecond QD PL decay can only result from FRET-sensitization. The QDs had a native PL lifetime of ca. 50 ns, following direct optical excitation (see Figure 4E); however, with assembly of PEB B−Tb, the QD manifested a 120 ± 30 μs PL lifetime that was significantly increased (∼2400-fold) and commensurate with the fast Tb PL decay component. Figure 4F shows plots of the Tb-sensitized, QD acceptor PL decays at the same ratios of PEP B−Tb used in Figure 4C and D. This result was conclusive evidence of the $FRET_1$ pathway and corresponded to an efficiency of 95 ± 3%, which was in good agreement with that estimated from the Tb PL decay. Assuming a $FRET_1$ efficiency between 91−98%, the Tb−QD center-to-center separation distance in $(PEP\ B{-}Tb)_n$−QD conjugates was calculated to be between 5.3 and 6.9 nm (6.3 nm for the median 94.5% efficiency). This value was also in good agreement with the estimated length of PEP B plus the QD radius (∼6.7 nm), despite the intrinsic insensitivity of FRET to changes in donor−acceptor separation distance at very high efficiencies.

QD-to-A647 Energy Transfer ($FRET_2$). We next examined the second QD-to-A647 energy transfer ($FRET_2$) step in the FRET relay. Increasing ratios of A647-labeled PEP A (PEP A−A647) were self-assembled around the central QD, and the nongated and time-gated PL emission spectra were measured. As shown in Figure 5A, increasing the ratio of assembled PEP A−A647/QD resulted in the progressive quenching of QD PL and sensitization of A647 PL via $FRET_2$ in the nongated PL spectrum. Analogous measurements of equivalent amounts of

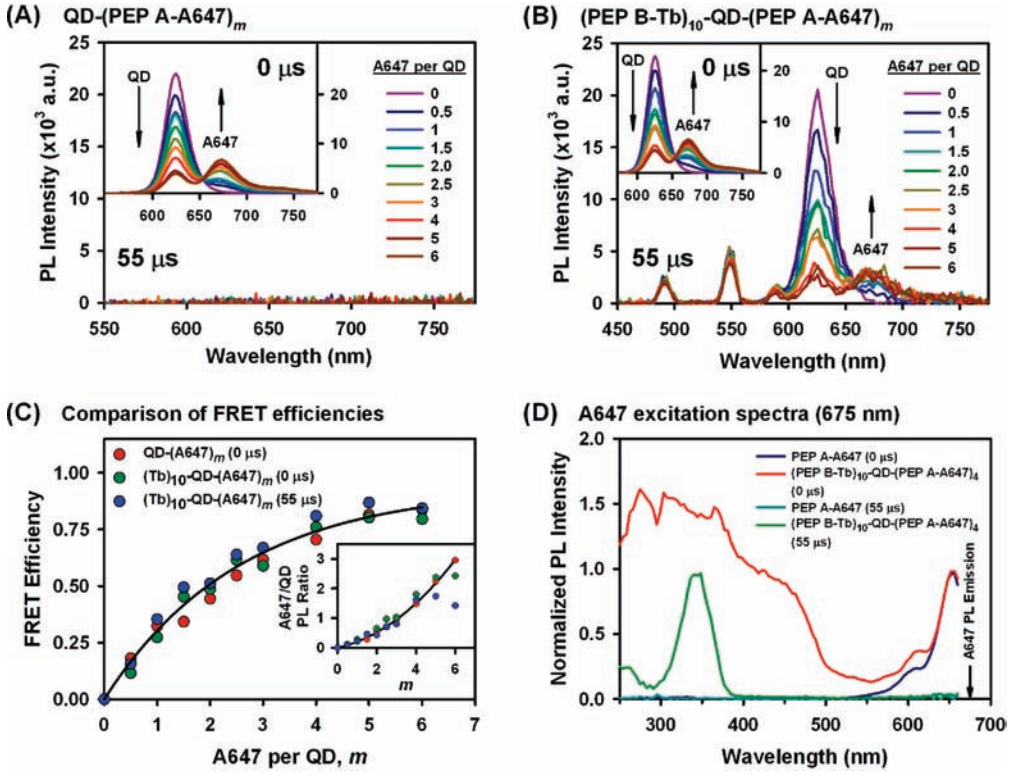

Figure 5. (A) Nongated (~0 μs) and time-gated (55 μs) PL spectra for QD−(PEP A−A647)$_m$ assemblies with increasing A647 valence (m). No PL was observed in the time-gated spectrum. (B) PL spectra of (PEP B−Tb)$_{10}$−QD−(PEP A−A647)$_m$ assemblies. QD and A647 PL are apparent in both the nongated and time-gated spectra. (C) Correlation of the FRET efficiencies as a function of A647 valence between the three different sets of PL spectra in parts A and B, calculated from the degree of QD donor quenching. The inset shows the corresponding A647/QD PL ratios. (D) A647 PL excitation spectra for the different configurations, illustrating both FRET$_1$ and FRET$_2$ sensitization.

PEP A−A647 without QD revealed negligible directly excited acceptor emission (data not shown), confirming efficient FRET and significant re-emission by the acceptor. The observed trends of increasing donor/acceptor quenching/sensitization were analogous to those observed with other QD donor−multiple dye acceptor FRET pairs.[20,35−38] Importantly, the time-gated PL spectrum of these conjugates revealed only background noise and no traces of QD or A647 PL. Fitting the nongated FRET data with the Förster model (eq S5, Supporting Information) yielded an average donor−acceptor separation of $r \approx 8.4$ nm for the QD−(PEP A−A647)$_m$ conjugates. This value was in good agreement with our predictions. In addition to a QD radius of ~5.5 nm, PEP A comprised a Pro$_7$ motif that forms a type-II helix ~1.2 nm in length[39] and 15 additional residues that contribute 1−1.5 nm of length. The overall separation was thus $r \approx 7.7$−8.2 nm. The maleimido linker in the dye structure will also contribute some extra length. Based on an average $r \approx 8.3$ nm (*vide infra*) and an intrinsic QD lifetime of 50 ns, the rate of FRET$_2$ was estimated at 1.1×10^7 s^{-1} per acceptor. This rate corresponds to ca. 36% FRET efficiency for the first A647 acceptor.

Tb-to-QD-to-A647 Time-Gated FRET Relay (FRET$_1$ + FRET$_2$). For the next FRET characterization, PEP B−Tb and PEP A−A647 were coassembled around the central QD to yield the final Tb-to-QD-to-A647 energy transfer relay. Time-gated PL measurements were again critical for observing Tb-sensitization of the QD during FRET$_1$ and the subsequent energy transfer from the QD to the A647 in FRET$_2$. To allow simple resolution of the effect of FRET$_1$ on FRET$_2$, the PEP B−Tb/QD ratio was fixed at an intermediate value of 10. This valence corresponded to a significant rate of QD sensitization (see Figure 3) while still leaving a large amount of the QD surface available for assembling PEP A−A647, which was added at ratios between 0 and 6 PEP A−A647/QD. As shown in the inset of Figure 5B, the nongated PL emission spectrum of the full conjugate revealed the QD PL quenching and sensitization of A647 PL characteristic of directly excited FRET$_2$ and similar to that of QD with only A647 shown in Figure 5A. Indeed, the data in the Figure 5A and B insets are almost superimposable, and analysis (eq S5, Supporting Information) yielded an estimated QD−A647 separation of $r \approx 8.3$ nm in the (PEP B−Tb)$_{10}$−QD−(PEP A−A647)$_m$ conjugates without time-gating—a value that deviated less than 2% from that measured for the nongated QD−(PEP A−A647)$_m$ conjugates (see Table 2). Coassembly of ~10 PEP B−Tb on the central QD thus had little effect on the directly excited FRET$_2$ pathway.

Figure 5B shows the time-gated PL emission spectra of the (PEP B−Tb)$_{10}$−QD−(PEP A−A647)$_m$ conjugates. In addition to Tb PL, both QD and A647 PL were observed. Even with sensitization from the FRET$_1$ pathway rather than direct optical excitation, the QD PL showed the same progressive quenching with an increasing ratio of PEP A−A647 acceptor/QD. Similarly, the A647 showed a corresponding pattern of FRET$_2$-sensitized PL that increased with its valence. Notably, the Tb PL was not significantly quenched by the addition of PEP A−A647, underlining the approximate independence of FRET$_1$ and FRET$_2$. Analysis of the time-gated QD PL quenching derived an average QD−A647 separation of $r \approx 8.1$ nm—a less than 3% deviation from the other two data sets (see Table 2). These two results confirmed that the

dx.doi.org/10.1021/ja210162f | J. Am. Chem.Soc. 2012, 134, 1876−1891

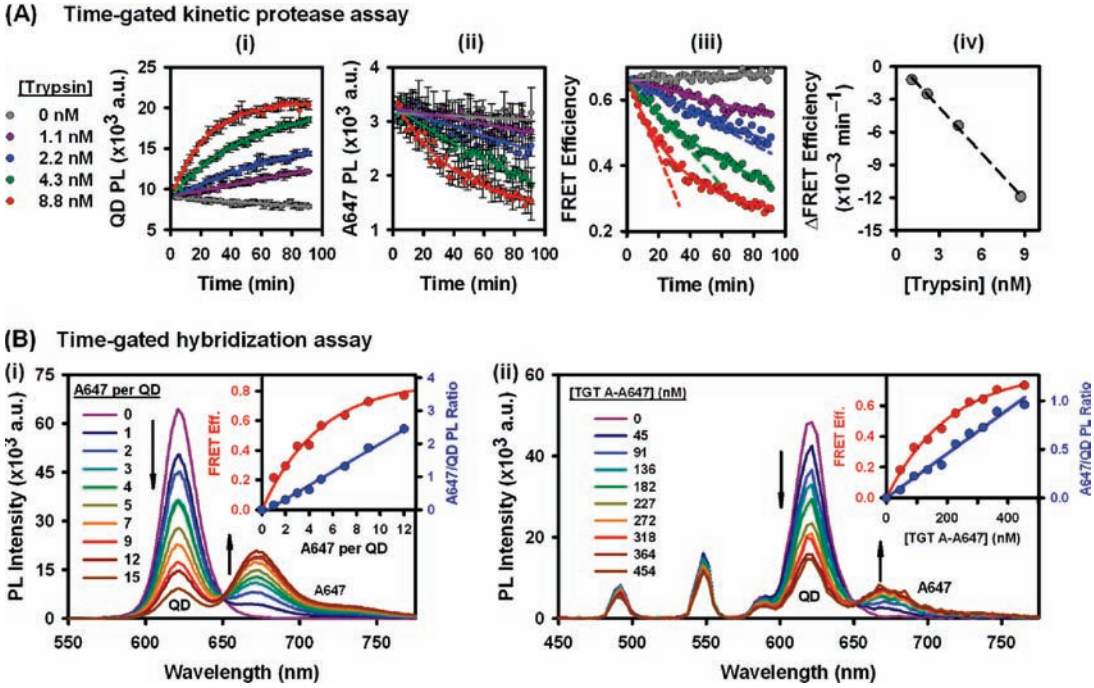

Figure 6. Time-gated biosensing configurations with a two-step QD-FRET relay. (A) Time courses of trypsin proteolytic activity using (PEP B–Tb)$_{10}$–QD–(PEP A–A647)$_3$ assemblies. The time-gated (i) QD and (ii) A647 PL were monitored and converted to (iii) FRET efficiency. Dashed lines represent tangents drawn to calculate the initial rate. (iv) Initial rate of change of FRET efficiency was proportional to the trypsin concentration. (B) (i) PL spectra for the nongated calibration of TGT A–A647 hybridization using QD–(PRB A)$_{15}$ assemblies. The inset shows the FRET efficiency and A647/QD PL ratio as a function of TGT A–A647/QD. (ii) Time-gated sensing of TGT A–A647 using (PEP B–Tb)$_{10}$–QD–(PRB A)$_{12}$ assemblies. The inset shows the FRET efficiency and A647/QD PL ratio as a function of TGT A–A647 concentration. Note: the corresponding TGT A–A647 added is given in equivalents in part i and concentration in part ii.

intrinsic properties of FRET$_2$ were carried over into the time-gated measurements sensitized by FRET$_1$. All three data sets are quantitatively compared in Figure 5C; they match extremely well and can all be fit to the Förster formalism. The average QD–A647 separation across the three data sets was $r \approx 8.3$ nm. Moreover, separate analysis of the FRET efficiency at each A647 valence across all three QD-to-A647 data sets yielded, on average, a relative standard deviation of <10%. In addition, the A647/QD acceptor/donor PL ratio was also determined and compared between the same data sets. A good correspondence is seen across the different PEP A–A647 valences, except for small negative deviations in the time-gated data at 5–6 PEP A–A647 per QD. We attribute the latter to poorer instrumental signal-to-noise (S/N) at the A647 wavelengths within the time-gated measurement settings, rather than a modification of FRET$_2$ (similarly, S/N is poorer for Tb in nongated measurements; see Figure S4 in the Supporting Information). This data also suggested that there was no significant "extra" sensitization of the A647 via direct Tb-to-A647 FRET, in agreement with our *a priori* expectations based on relative energy transfer rates.

To further establish the FRET$_1$ + FRET$_2$ relay, excitation spectra were collected with PEP A–A647 and (PEP B–Tb)$_{10}$–QD–(PEP A–A647)$_4$ conjugates, as shown in Figure 5D. The PEP A–A647 valence was fixed at 4 per QD to ensure efficient but nonsaturated FRET. The excitation spectra were collected at 675 nm, corresponding to A647 PL emission. PEP A–A647 alone was characterized by its own excitation/absorption profile without time-gating and gave rise to no measurable excitation spectrum with time-gating. In contrast, the (PEP B–Tb)$_{10}$–QD–(PEP A–A647)$_4$ conjugate excitation spectrum was a composite of the A647 and QD excitation/absorption profiles without time-gating. This was indicative of direct excitation and FRET$_2$, respectively. Importantly, with time-gating, the excitation spectra corresponded to that of the Tb, unequivocally demonstrating that the time-gated sensitization of the A647 originated from the Tb via consecutive FRET$_1$ and FRET$_2$ processes at the QD. Cumulatively, the data collected to this point also suggested that FRET$_1$ and FRET$_2$ were approximately independent of one another (time-gated sensitization notwithstanding).

Proteolytic Assays. The first biosensing configuration investigated with the energy transfer relay was protease sensing in a time-gated, kinetic mode. We utilized PEP A–A647 and PEP B–Tb along with trypsin—a prototypical serine protease that cleaves on the C-terminal side of arginine and lysine residues. To enable sensing, PEP A incorporated one lysine (K) and two arginine (R) cleavage sites along its length.[40] In contrast, PEP B contained no lysine or arginine residues and was therefore not a potential substrate for trypsin (confirmed experimentally; data not shown). The time-gated QD–FRET relay monitored trypsin activity by following the loss of FRET$_2$ from proteolysis of PEP A–A647. Analogous to previous QD–FRET configurations for sensing proteolytic activity,[36,38,40] the initial state of our time-gated configuration was "ON" with respect to the QD–A647 FRET$_2$ pair, as illustrated in Figure 1B (i). Proteolysis decreased the number of A647 proximal to the QD, progressively shifting the system toward a FRET$_2$ "OFF" state with increasing activity, and thus provided a dynamic signal. In parallel, PEP B–Tb provided approximately constant time-gated sensitization of the QD by FRET$_1$. We chose to use (PEP B–Tb)$_{10}$–QD–(PEP A–A647)$_3$ conjugates

dx.doi.org/10.1021/ja210162f | J. Am. Chem.Soc. 2012, 134, 1876–1891

because 10 equiv of PEP B−Tb provided significant time-gated QD sensitization, and 3 initial equivalents of PEP A−A647 afforded maximal changes in FRET efficiency during subsequent proteolysis. Importantly, and in contrast to previous configurations, we were able to implement time-gated sensing as a result of the $FRET_1$ pathway. Another novel feature was the measurement of protease activity in a kinetic mode, where the course of proteolysis was followed in real-time using two-color ratiometric measurements.

As shown in Figure 6A, exposing the FRET-relay protease sensor to increasing amounts of trypsin increased the rate at which FRET-sensitized QD PL recovered and the rate at which $FRET_2$-sensitized A647 PL was lost. Accordingly, the time-dependent $FRET_2$ efficiency showed a commensurate decrease with the progression of proteolysis. The initial rate of change in the $FRET_2$ efficiency also increased linearly with increases in protease concentration. Control experiments with no trypsin showed consistent QD PL, A647 PL, and FRET efficiency over all time courses. For the unoptimized combination of QD−peptide substrate concentrations, trypsin preparation, sample conditions, and analysis time utilized herein, we estimated a limit of detection (LOD) of 200 pM (0.5 ng) trypsin (using a threshold value of three standard-errors beyond the slope of the line of best fit through the FRET efficiency time course for the negative control at 0 nM trypsin). This LOD represents an approximately 3-fold and 30-fold improvement compared to the 625 pM or 6.25 nM previously estimated for a similar QD−FRET sensor assembled using the same peptide substrate (with smaller QDs and a different acceptor dye) but measured in a nonkinetic mode on a fluorescent plate reader or a custom microchip platform, respectively.[40,41] The improvement in LOD was somewhat remarkable, given that the previous studies used QD−FRET sensors based on a single QD-to-dye FRET pathway. However, in our FRET relay, the efficiency of $FRET_1$ was very high (∼94%), which minimized the loss of final acceptor sensitization due to the added energy transfer step. We also attribute the increase in sensitivity to the added kinetic analysis, which allows greater resolution of low activity proteolysis.

Time-Gated DNA Hybridization Assay. The second sensing configuration explored using the FRET relay was a time-gated hybridization assay. To this end, we used QDs coassembled with PEP B−Tb and PRB A. Initial measurements were made without time-gating by mixing QDs with 15 equiv of PRB A that had been prehybridized with increasing amounts of TGT A−A647, as a QD-$(PRB\ A)_{15}$/$(TGT\ A{-}A647)_m$ configuration. As shown in Figure 6B (i), the result was the expected rise approaching maximum FRET efficiency and an approximately linear increase in the FRET-sensitized A647/QD PL ratio. The latter provided a more convenient (linear and no reference state needed) and sensitive capacity for quantitative detection. For the time-gated hybridization assay, $(PEP\ B{-}Tb)_{10}$−QD conjugates were coassembled with 12 equiv of PRB A to detect an increasing quantity of TGT A−A647, as shown in Figure 1B (iii). Analogous to the time-gated protease construct, the role of PEP B−Tb was to provide time-gated sensitization of the QD PL in the final $(PEP\ B{-}Tb)_{10}$−QD−$(PRB\ A)_{12}$/$(TGT\ A{-}A647)_m$ configuration. The latter time-gated PL spectrum revealed the expected FRET "ON" progression as the amount of hybridized TGT A−A647 increased, indicated by decreases in QD PL and corresponding increases in sensitized A647 PL. Between the nongated and time-gated formats, the $FRET_2$ efficiency, as a function of the number of equivalents of PEP A−A647, did not change (see Figure 6B and Figure S8 in the Supporting Information); however, the slope of the A647/QD PL ratio diminished, which we again attributed to lower signal-to-noise for the A647 PL within the time-gated measurements. Quantitative time-gated data (Figure 6B (ii)) was obtained from the linear increase in A647/QD PL ratio, and the LOD was estimated to be 16 nM (1.8 pmol). The LOD threshold, determined at ca. 670 nm, was set as three standard deviations above the average baseline QD PL spectrum in the region 660−775 nm (see eqs S22 and S23 in the Supporting Information). That is, the minimum amount of TGT A−A647 needed to have a reliably measurable A647 PL signal above the noise expected due to the QD crosstalk at ca. 670 nm, and with which to calculate an A647/QD PL ratio. While we did not investigate the upper limit of the dynamic range of the assay, a continuation of the linear trend in A647/QD PL ratio was noted at a 25% excess of TGT A−A647 over PRB A (data not shown), suggesting that probe-target hybridization was less than 1:1. In terms of concentration, the 16 nM LOD was approximately 1 order of magnitude higher than the ∼1 nM LODs previously reported for ensemble solution-phase[42] and solid-phase hybridization assays[43] based on QD-dye FRET pairs (no relay). Those assays used 500 and 1250 μL sample volumes (cf. 100 μL used herein), such that the LOD in terms of the absolute quantity of material was comparable (∼0.5−1.3 pmol). However, as a ratiometric measurement, it should be noted that this value is a function of both the QD-bioconjugate concentration and sensitivity of the instrumentation. In our experiments, the limitation appeared to be the microplate reader, which was primarily designed for high-throughput analysis instead of high sensitivity spectrofluorimetry, and prevented the use of lower quantities of QD to detect smaller amounts of target. Nevertheless, these results confirmed that DNA hybridization could also be monitored using time-gated Tb-to-QD-to-A647 FRET.

Orthogonal Two-Plex DNA Hybridization Assay. The last sensing configuration we implemented focused on exploiting the approximately independent $FRET_1$−$FRET_2$ mechanisms for signal transduction in a multiplexed format. The results presented thus far have clearly demonstrated that the two different energy pathways could be increasingly sensitized by the assembly of more Tb or A647 per QD. In contrast to previous QD-based biosensing formats,[44] this unique feature provides a route to multiplexed detection that does not derive its information from the use of multiple QD colors but rather from the temporal resolution of the $FRET_1$ and $FRET_2$ processes. Our goal was to demonstrate that each FRET process could reflect a distinct biorecognition event and provide an orthogonal analytical signal.

We have shown that the magnitude of $FRET_1$-sensitized time-gated QD PL is linearly proportional to the amount of proximal Tb (see Figure 3). Likewise, the A647/QD PL ratio can be linearly proportional to the amount of proximal A647 (see Figure 6B). For a two-plex assay, it was clear that the nongated A647/QD PL ratio would reflect $FRET_2$ uniquely because the Tb signal is excluded from these measurements. Thus, any biomolecular binding event associating A647 with the QD could be detected orthogonally to any events associating the Tb with QD. We also realized that the time-gated QD PL sensitization could be used to measure the extent of $FRET_1$ but only if we accounted for the quenching effect of proximal A647. Thus, we used the total time-gated QD + A647 PL sensitization as an analytical signal for the extent of the

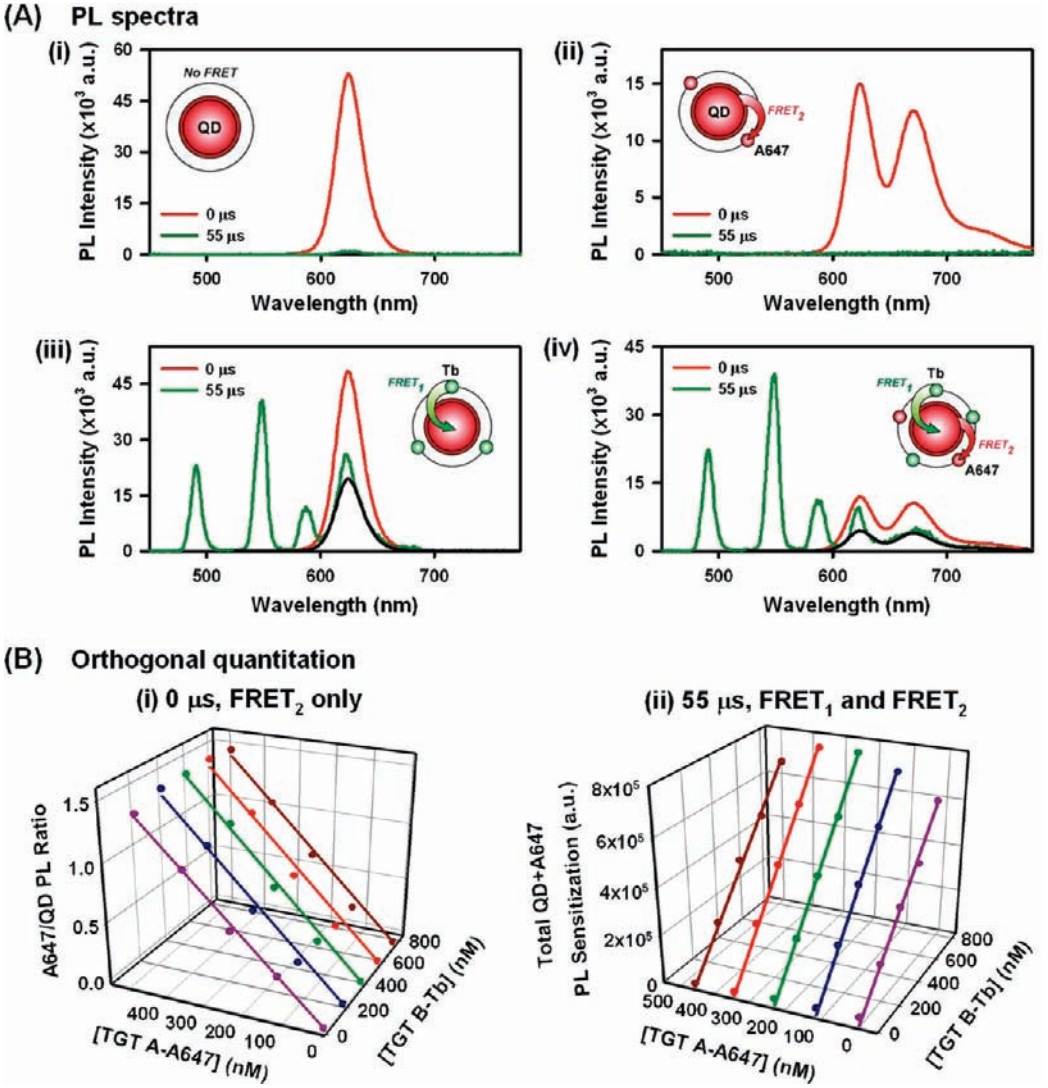

Figure 7. Time-gated two-plex sensing of nucleic acid hybridization using a two-step QD-FRET relay. (A) PL spectra showing the characteristic nongated (~0 μs) and time-gated (55 μs) response of $(PRB\ B)_{16}$–QD–$(PRB\ A)_{10}$ assemblies: (i) no target; (ii) TGT A–A647; (iii) TGT B–Tb; and (iv) TGT A–A647 and TGT B–Tb. The solid black lines show scaling of the nongated PL spectrum to fit the time-gated PL spectrum (via numerical deconvolution). (B) Orthogonal calibrations curves based on measurement of (i) the nongated A647/QD PL ratio and (ii) time-gated total QD+A647 PL sensitization. Each parameter responded linearly to increasing amounts of the corresponding target and was approximately independent of the other analytical parameter.

$FRET_1$ process. A correction based on the A647 quantum yield (see eq S7 in the Supporting Information) was introduced to account for energy that was transferred from the QD but was not re-emitted by A647. This analysis provided a working model and two predicted orthogonal analytical signals to verify experimentally. A DNA hybridization assay was selected because Watson–Crick base-pairing is a selective biorecognition event that can be readily designed to avoid cross-reactivity.

In conjunction with nongated and time-gated measurements, a two-plex configuration was created by assembling $(PRB\ B)_{16}$–QD–$(PRB\ A)_{10}$ conjugates to respond to TGT B–Tb and TGT A–A647. The oligonucleotides were prehybridized with target, the QDs added, and self-assembly allowed to occur yielding $(TGT\ B–Tb)_n$/$(PRB\ B)_{16}$–QD–$(PRB\ A)_{10}$/$(TGT\ A–A647)_m$ conjugates for detection. Figure 1B (ii) illustrates the generic bioconjugate structure, while the schematics in Figure 7A depict the different permutations of target hybridization-mediated FRET within the bioconjugates at the four extremes of the assay: $m = n = 0$; $m = 10$, $n = 0$; $m = 0$, $n = 16$; and $m = 10$, $n = 16$ (see also Figure S9 in the Supporting Information). The first permutation (i) corresponded to an absence of target and only the QD, which gave rise to QD PL without time-gating, and no signal with time-gating. Permutation (ii) corresponded to the hybridization of TGT A–A647, which resulted in a mixture of QD and $FRET_2$-sensitized A647 PL in nongated measurements, and no signal in time-gated measurements. The third permutation (iii) corresponded to the hybridization of TGT B–Tb, which yielded only QD PL without time-gating, and a mixture of Tb and $FRET_1$-sensitized QD PL with time-gating. Finally, permutation (iv) corresponded to hybridization of both TGT A–A647 and TGT B–Tb. Here, the nongated spectrum showed QD and $FRET_2$-sensitized A647 PL, whereas the time-gated spectrum showed Tb PL, $FRET_1$-sensitized QD PL and $FRET_2$-sensitized A647 PL, reflecting assembly of the full Tb-to-QD-to-A647 FRET relay.

The orthogonality of the two-plex hybridization assay was evaluated using an array of different mixtures of TGT A–A647

dx.doi.org/10.1021/ja210162f | J. Am. Chem.Soc. 2012, 134, 1876–1891

and TGT B−Tb (see Table S5 in the Supporting Information), followed by calculation of the nongated A647/QD PL ratio ($FRET_2$) and time-gated total QD + A647 PL sensitization ($FRET_1$) from the measured PL spectrum of each mixture. As the amount of TGT A−A647 increased, the nongated A647/QD PL ratio increased linearly, but was relatively unaffected by the presence or absence of TGT B−Tb (Figure 7B (i)). Similarly, as the amount of TGT B−Tb increased, the total QD + A647 PL sensitization increased linearly, but it was minimally affected by changes in the presence of TGT A−A647 (Figure 7B (ii)). It is important to note that the data in Figure 7B (i and ii) were collected simultaneously in the same experiment and from the same samples. These results effectively demonstrated orthogonal quantitative responses, where the A647/QD PL ratio responded to TGT A−A647, and the total QD + A647 PL sensitization responded to TGT B−Tb. For a rigorous demonstration of the concept and analysis, we took steps to numerically deconvolve the small amount of overlapping Tb PL from the QD PL in the measured two-plex PL spectra (alternative analyses are discussed later). The LOD for TGT A−A647 and TGT B−Tb were estimated to be 17 nM (1.9 pmol) and 29 nM (3.2 pmol), respectively. The LOD thresholds were taken as three standard deviations above the average A647/QD PL ratio (0 nM TGT A−A647, 0−727 nM TGT B−Tb, time-gated) or total QD + A647 PL sensitization (0 nM TGT B−Tb, 0−454 nM TGT A−A647, nongated). Despite the two-plex format, these LODs compare favorably to our time-gated, one-plex hybridization assay.

DISCUSSION

QD Nanoplatform. Several properties of the 625 nm PL QDs were uniquely advantageous for assembling the two-step energy transfer relay—particularly when acting as an intermediary. The strong, broad QD absorption was resonant with the three strongest Tb emission lines and was characterized by extinction coefficients approaching 1 order of magnitude greater than that of most fluorescent dye acceptors.[45] The use of a fluorescent dye intermediary in our FRET relay configuration would also be hindered by a narrower absorption band that would only be resonant with two of the Tb emission lines. As a consequence, the QD acceptor offered a much larger spectral overlap integral and Förster distance with the Tb. The QD PL was also well separated from the Tb PL (except for the Tb emission line at 620 nm, which was the least intense of all the lines). In turn, when the QD functioned as the donor for the final A647 acceptor in the relay, the narrow QD PL provided strong overlap with the A647 absorption, while its peak remained spectrally well-resolved from the A647 emission at 675 nm. The latter would not have been possible with a fluorescent dye intermediary given the characteristic broad and red-tailed dye emission profile.

The nontrivial surface area of the QD was of almost equal importance to its optical properties, and its utilization as a central nanoscaffold greatly facilitated the physical assembly of the energy transfer relay. In contrast, the use of a fluorescent dye intermediary in the relay would require an extrinsic scaffold, such as a protein or double-stranded DNA, to provide the necessary proximity with the initial donor(s) and final acceptor(s). Such a scaffold would not readily provide the approximately centrosymmetric distribution of Tb and A647 that was achieved with the QD intermediary, and which enabled straightforward analysis. Further, because the QD was its own intrinsic scaffold, it enabled the use of peptides and nucleic acids in a biological rather than structural motif. A maximum of 20 total peptides (PEP A + PEP B) were assembled per QD here, which is less than half of the maximum packing expected for even smaller QDs.[32] This "extra" surface availability could allow the assembly of one or more other biomaterials to the QD in order to provide utility beyond the FRET relay. For example, cell penetrating or other targeting peptides could be added to induce cellular uptake or *in vivo* targeting of the final bioconjugate.[46−51]

It must also be noted that the properties of His_6 self-assembly were equal in importance to the properties of the QD as a nanoscaffold and luminophore. The principle benefits of utilizing the His_6 motif were its simplicity, efficiency, and reproducibility. QD bioconjugation required only mixing of the QD and the desired equivalents of biomolecule(s). This level of control over QD-bioconjugate valence effectively permitted tuning of the relative efficiency of the $FRET_1$ and $FRET_2$ pathways, regardless of the use of Tb/A647 labeled His_6-appended peptides, or His_6-appended oligonucleotide probes hybridized with labeled target. Such versatile and incremental tuning of two distinct FRET pathways—solely through assembly valence—may be unique to the use of QDs and His_6-bioconjugation in these types of assemblies. In contrast, we have shown that assembling biotinylated DNA to streptavidin-coated QDs results in a large amount of heterogeneity in separation distance, hindering control and characterization of FRET.[34] Purely synthetic chemical approaches to deriving similar architectures based on, for example, a dendrimeric substrate, are extremely labor intensive, and neither spin coating nor layer-by-layer approaches would provide the same levels of control and/or precision as His_6.[17,52]

Tb Donors and the QD Acceptor in $FRET_1$. Insight into the initial Tb-to-QD FRET process was provided by examining the stepwise, concentric assembly of labeled-peptide around the central QD scaffold. Notably, increasing the amount of PEP B−Tb per QD monotonically increased the time-gated QD PL intensity, and did not show the saturation typical of FRET pairs with QD donors. To help interpret this data, we use the more familiar "single QD donor−multiple acceptor" FRET system as a reference point.[5,8,37] Consider the effect of assembling multiple acceptor dyes around a central QD donor (e.g., $FRET_2$): more dye acceptors increase the FRET-sensitization of dye PL, and do so by increasing the probability of a one-time, single quantum energy transfer event from the excited QD to an arbitrary, proximal dye acceptor (FRET efficiency increases). Across the ensemble, the number of FRET-sensitized dye molecules increases; however, at the level of single FRET pairs, and regardless of the number of dyes assembled per QD, only one dye molecule can be sensitized each time an assembly is excited at the QD. On the other hand, the effect of assembling more Tb donors around a central QD acceptor is, *a priori*, far more complex. As a result of the ca. 3 orders of magnitude difference between the FRET-related Tb lifetime and the intrinsic QD lifetime, there is potential for multiple quanta of energy (i.e., multiple excited-state Tb donors) within a single assembly. Assembly of multiple Tb donors does not increase the probability of a one-time, single quantum energy transfer from any one arbitrary Tb donor to the QD (FRET efficiency is unchanged). It does, however, increase the probability that the QD will accept energy via FRET, as more excited Tb is assembled (i.e., the QD becomes brighter as more Tb is assembled).[33] With only 2 or 3 Tb donors per QD, the probabilities of transfer of at least one energy quantum to the

QD are >99% and >99.9%, respectively, although the probability for transfer from one particular Tb donor remains ~94−95%.

It is also instructive to examine the conditions that effectively guaranteed time-gated sensitization of the QD via $FRET_1$. While 2−3 excited-state Tb donors per QD should ensure energy transfer to the QD (>99% probability), mixing 2 equiv of PEP B−Tb per QD does not ensure that every QD is conjugated with 2 Tb donors. Based on self-assembly that follows a Poisson distribution process,[53] a ratio of 7:1 PEP B−Tb/QD must be added to ensure that >99% of the individual QDs in the ensemble have ≥2 PEP B−Tb assembled. Furthermore, within the 1 ms PL measurement integration time, ca. 32% of the Tb donors ($\tau \sim 2.6$ ms) will have returned to their ground state via intrinsic relaxation pathways following flash excitation. Thus, an average of at least 10 PEP B−Tb/QD is needed for >99% of the QDs to have two proximal excited-state Tb donors over the full integration time (and hence our use of this valence in biosensing experiments). Further still, the dissociation constant for His_6-QD assembly is ~1 nM.[31] At the 50 nM QD concentrations used in most steady-state experiments, and for 1−20 added equiv of PEB B−Tb, we estimated that between 13−4%, respectively, of the added PEP B−Tb were unbound. A targeted valence of ca. 11 would be needed to ensure the binding of 10 equiv of PEB B−Tb. It is also improbable that each Tb in a QD-bioconjugate was simultaneously excited at the low power densities used herein; therefore, even more than 11 Tb equiv must be added to guarantee a more than 99% energy transfer efficiency to the QD via $FRET_1$. While these considerations provide a viable basis for the observation of increased QD PL sensitization with increased Tb/QD, there is also a photophysical consideration: the rate of $FRET_1$ (6.6×10^3 s^{-1}) is 17-fold faster than the intrinsic decay of the Tb excited state (3.9×10^2 s^{-1}), and both these rates are dramatically slower than the decay of the QD excited state (2.0×10^7 s^{-1}). Thus, a QD can potentially accept a quantum of energy from a proximal Tb donor, return to its ground state, and repeat this process many times over a 1 ms integration time if there are multiple proximal Tb donors. We assume that the observed increase in time-gated QD sensitization at ratios >11 PEB B−Tb/QD were due to excitation of a larger number of proximal Tb/QD, combined with the possibility of successive $FRET_1$ events.

A curious aspect of the Tb-to-QD $FRET_1$ process was the two-component Tb PL decays, where one component was a FRET quenched lifetime and the other was residual native Tb lifetime. This result suggested two distinct populations of Tb: one that engaged in efficient FRET with the QD and one that did not. We suggest that this dichotomy was at least partly due to a fraction of PEB B−Tb that was not bound to QDs (perhaps the 4−13% noted above).

Energy Flow through the Time-Gated FRET Relay. We have demonstrated that each individual step in the FRET relay was very efficient, and we now consider the net energy transfer through the contiguous system. Energy flow starts at the first internal energy transfer within the Tb complex. The total Tb luminescence QY is the product of the transfer efficiency from the light absorbing ligand to the central Tb^{3+} ion and the QY of the central Tb^{3+} ion ($\Phi_{tot} = \Phi_{trans} \times \Phi_{Tb}{}^{3+}$).[54] Given Φ_{tot} = 60% (Lumiphore) and Φ_{Tb} = 77% (Table 2), it follows that Φ_{trans} = 78%. Therefore, 78% of the energy absorbed by the complex arrived at the central Tb^{3+} ion, and approximately 77% was not lost as heat. Of this, 94% was transferred to the QD via $FRET_1$, such that there was a maximum of 56% excitation energy transfer efficiency ($= \Phi_{trans} \times \Phi_{Tb} \times E_{FRET_1} = 0.78 \times 0.77 \times 0.94$; that is, excitation events at the Tb that result in QD excitation). In turn, the QD had a 55% QY for a 31% emission transfer efficiency ($= \Phi_{trans} \times \Phi_{Tb} \times E_{FRET1} \times \Phi_{QD} = 0.56 \times 0.55$; that is, excitation events at the Tb that result in QD emission) through $FRET_1$. Adding the time-gated $FRET_2$ pathway, which occurred with ~83% efficiency at 5−6 PEP A−A647/QD, the excitation transfer efficiency to the A647 was 26% ($= \Phi_{trans} \times \Phi_{Tb} \times E_{FRET_1} \times \Phi_{QD} \times E_{FRET_2} = 0.31 \times 0.83$). Because $\Phi_{A647} \approx 0.33$, the emission transfer efficiency was estimated as 9% ($= \Phi_{trans} \times \Phi_{Tb} \times E_{FRET_1} \times \Phi_{QD} \times E_{FRET_2} \times \Phi_{A647} = 0.26 \times 0.33$). Previously, a ~5% end-to-end transfer efficiency was reported for a structurally similar two-step, multivalent FRET relay using an initial QD donor with Cy3 intermediaries and terminal Cy5 acceptors along a DNA scaffold.[23] The enhancement in net efficiency in the current relay—despite the presence of three-underlying ET steps (ligand−Tb^{3+}−QD−A647)—highlights the advantage of using a QD as an intermediary due to its unique optical properties and nanoscaffold capability.

Another point of interest was the possibility that efficient $FRET_2$ might be able to increase the net rate of $FRET_1$ to the QD (the rate of $FRET_1$ from one particular Tb donor is fixed). That is, the possibility that faster decay of the QD excited-state with increasing $FRET_2$ can pull or "siphon" energy from the Tb donors at a faster rate. While this phenomenon may be possible in certain FRET relay systems, it was improbable in our configuration. The rate of $FRET_1$/Tb was more than 1700-fold slower than the rate of $FRET_2$/A647, with $FRET_1$ occurring over the time scale of hundreds of microseconds compared to tens of nanoseconds for $FRET_2$. The limiting rate was thus that of $FRET_1$, precluding any siphoning effect by $FRET_2$.

Time-Gated Biosensing. With few exceptions, multistep FRET relays incorporating QD-bioconjugates have been based on QD-to-dye-to-dye energy transfer configurations.[20−22] The role of the relay in these instances was primarily to extend the range of energy transfer and/or to allow for wavelength shifting. Herein, the former consideration was addressed by the large Förster distances of the $FRET_1$ (10.1 nm) and $FRET_2$ (7.5 nm) pairs, while the latter was addressed by pairing a red-emitting QD with the deeper-red A647 acceptor. The unique features of the Tb-to-QD-to-A647 FRET relay were the added ability to make time-gated QD PL measurements, and sensitization of QD-to-A647 energy transfer over a millisecond time scale. With time-gating, any undesirable direct excitation of the final A647 acceptor—regardless of the excitation wavelength used—was completely avoided because of its ~1 ns fluorescence lifetime.[55] However, a potentially more important advantage arises from the <20 ns characteristic decay times of cellular and tissue autofluorescence,[56] such that the time-gating afforded by Tb-to-QD FRET is expected to permit the separation of analytical PL signals from unwanted background PL in almost any complex biological matrix. While the protease sensing demonstrated in this work was primarily proof-of-concept for demonstrating utility of the FRET relay, it should be noted that abnormal protease activity is associated with many diseases, including ischemia, autoimmune and neurodegenerative disease, and several types of cancers.[57] This relevance suggests, for example, the possibility of sensitive, time-gated, *in situ* measurements of protease activity associated with overexpressed extracellular matrix metalloproteinases in complex tumor milieu. Use in

complex biological matrices will be predicated on the fidelity of the QD-conjugate assemblies therein. Complexation of the Tb is highly stable and selective for lanthanide ions,[28] polyhistidine is not an endogenous motif, and PEG coatings are largely biocompatible[24,58,59]—all of which suggest that preassembled QD-conjugates should remain functional in biological matrices.

In addition to the advantages of time-gating via the Tb−QD FRET pair, there are advantages associated with the ratiometric detection afforded by the QD−A647 FRET pair. Ratiometric analyses tend to be relatively insensitive to dilutions and small variations in excitation intensity or between different instruments. This format is also particularly well suited to assays in a kinetic format, where donor and acceptor PL intensities dynamically change over extended time periods (e.g., hours) and are highly susceptible to instrumental drift and noise.

Orthogonal Spectrotemporal Multiplexing. In previous FRET sensing configurations based on QD donors, multiplexed information has been encoded by using two different colors of QD with either a common[60] or different FRET acceptors.[35] Multiplexing configurations where QDs have been used as FRET acceptors also rely on multiple QD colors.[11,14] In practice, ratiometric methods based on use of different fluorescent acceptor(s) have been preferred, and the number of colors measured (i.e., wavelength bands) was always greater than the number of targets. Moreover, multiplexing in these formats was usually limited to the ensemble because each individual QD-bioconjugate still only transduced one type of target. Compared to this state-of-the-art, the Tb-to-QD-to-A647 FRET relay offers an important and unique possibility in multiplexed bioanalysis: the ability to simultaneously transduce the activity of two different biomolecular targets by using a single color of QD in combination with orthogonal PL signals that are sensitive to different luminophores (the latter are bound to the QDs via biomolecular recognition). Furthermore, because these signals were proportional to the number of proximal acceptors, we were able to demonstrate the viability of this assay format in a semiquantitative, two-plex hybridization assay (Figure 7).

The use of full PL spectra and numerical deconvolution to resolve overlapping Tb and QD PL were necessary only for characterization and validation of the two-plex strategy. The small degree of Tb crosstalk in measuring QD PL only appeared in the time-gated measurement and systematically added to the apparent magnitude of the latter, such that it was readily calibrated into quantitative results (see Figure S10 in the Supporting Information). Alternatively, the use of 605 nm PL QDs, which would also be a suitable intermediary for the Tb and A647 in a relay, could potentially avoid this limited crosstalk because its PL maximum falls between the 585 and 620 nm Tb emission lines. In either case, the Tb PL intensity need not factor into the analysis, thereby permitting the use of two-color detection centered on the QD and A647 PL. Importantly, this two-color advantage does not come at the cost of ratiometric measurements. Because the A647 and QD PL manifests in both the nongated and time-gated PL spectra, the $FRET_1$ pathway can be measured relative to the directly excited $FRET_2$ pathway by dividing the time-gated A647 + QD PL sensitization ($FRET_1$ signal) by the nongated A647 + QD PL, which is a reference state independent of $FRET_1$ (see Figure S10 in the Supporting Information). Thus, both $FRET_1$ and $FRET_2$ can be analyzed ratiometrically. The caveat of this FRET-relay strategy is that only static biological processes, or those with slow dynamics ($\geq 10^{-2}$ s), can be monitored because of the need for microsecond time-gating and a millisecond integration time.

It should be noted that our spectrotemporal two-plex hybridization assay was primarily proof-of-concept, and not strictly biosensing *per se*, because labeled oligonucleotide targets were used in place of, for example, unlabeled genomically derived targets. Nevertheless, the orthogonal calibration curves in Figure 7B are a powerful confirmation of the approximate independence of the $FRET_1$ and $FRET_2$ pathways, as well as the strong biosensing potential of this time-gated, multiplexed FRET configuration. Dependence on directly labeled targets can be avoided by using labeled reporter oligonucleotides in a sandwich format,[43,61,62] intercalating dyes,[35,42,63] or molecular beacon configurations.[29,64,65] Simultaneous monitoring of two different proteases should also be feasible in this spectrotemporal format, as well as targeting of many other enzymatic processes.[14,66] An intriguing idea is utilizing the $FRET_1$ and $FRET_2$ processes to monitor and correlate physically associated, coupled, or cascaded events while still using a single QD assembly. For example, certain proteases have differential sensitivity to phosphorylated versus nonphosphorylated peptide substrates.[67] This capability could allow the correlation of kinase/phosphatase activity that is coupled to subsequent proteolysis. Beyond *in vitro* applicability, access to multiplexed sensing using a single compact QD-based probe can reduce the amount of extraneous material that must be delivered intracellularly. This feature potentially lessens the perturbation of a cellular system under study, and/or avoids challenges associated with differences in the cellular delivery efficiency between two distinct probes. It would also reduce some optical complexity in multiplexed microscopy systems (e.g., four color channels for two distinct donor−acceptor pairs without a relay, versus two color channels and electronics for time-gating when utilizing such a relay).

■ CONCLUSIONS

We have demonstrated the concentric coassembly of peptides and/or oligonucleotides labeled with Tb and A647 around a central QD nanoplatform to develop a time-gated Tb-to-QD-to-A647 FRET relay. The QD intermediary served simultaneously as both a donor and acceptor. The assembly of increasing amounts of Tb donor around the QD caused an approximately linear increase in the time-gated QD (acceptor) PL sensitization via $FRET_1$. Microsecond time-gating was necessary to observe $FRET_1$ because of the strong, direct optical excitation of the QDs and was enabled by the long Tb excited state lifetime. Time-gated PL lifetime measurements of both the Tb and QD indicated that the Tb-to-QD $FRET_1$ efficiency was ca. 94−95%. The addition of A647 acceptors to the QD (donor) yielded characteristic quenching of QD PL and $FRET_2$-sensitization of A647 PL. Equivalent $FRET_2$ efficiencies were observed with and without time-gated sensitization of the QD excited state via $FRET_1$. Detailed photophysical characterization confirmed the presence of the two FRET pathways and their approximate independence. The FRET relay was incorporated into model time-gated assays for protease activity and nucleic acid hybridization; the Tb-to-QD $FRET_1$ pathway sensitized time-gated PL and the QD-to-A647 $FRET_2$ pathway provided a ratiometric analytical signal proportional to biorecognition. Importantly, the FRET relay was applied in a novel two-plex nucleic acid hybridization assay, which highlighted the potential utility of a single color of QD bioconjugate functioning as a nanosensor capable of the

orthogonal, spectrotemporal detection of two different target sequences. When fully developed, such spectrotemporally resolved QD-FRET relays may have much to offer the field of bioanalysis.

■ ASSOCIATED CONTENT

Supporting Information

Detailed descriptions of reagents, labeling chemistry, bioconjugate and assay preparation, instrumentation, data analysis, equations for calculation of FRET efficiencies, FRET ratios, FRET rates, additional PL intensity and PL decay data, further discussion of peptide design, characterization of QD-oligonucleotide conjugates, further description of the two-plex hybridization assay, and alternate analysis methods. This material is available free of charge via the Internet at http://pubs.acs.org.

■ AUTHOR INFORMATION

Corresponding Author

E-mail: Igor.medintz@nrl.navy.mil.

■ ACKNOWLEDGMENTS

The authors thank Lumiphore, Inc. for providing the Lumi4−Tb complex and Invitrogen by Life Technologies for the QDs. The authors acknowledge DTRA, DARPA, ONR, NRL, the NRL-NSI, the European Commission (FP7 project NANOGNOSTICS), and the Innovative Medicines Initiative (IMI project OncoTrack) for financial support. W.R.A. is grateful to the Natural Sciences and Engineering Research Council of Canada (NSERC) for a postdoctoral fellowship.

■ REFERENCES

(1) Algar, W. R.; Susumu, K.; Delehanty, J. B.; Medintz, I. L. *Anal. Chem.* **2011**, *83*, 8826−8837.
(2) Rosenthal, S. J.; Chang, J. C.; Kovtun, O.; McBride, J. R.; Tomlinson, I. D. *Chem. Biol.* **2011**, *18*, 10−24.
(3) Gill, R.; Zayats, M.; Willner, I. *Angew. Chem., Int. Ed.* **2008**, *47*, 7602−7625.
(4) Hildebrandt, N. *ACS Nano* **2011**, *5*, 5286−5290.
(5) Medintz, I. L.; Mattoussi, H. *Phys. Chem. Chem. Phys.* **2009**, *11*, 17−45.
(6) Nabiev, I.; Rakovich, A.; Sukhanova, A.; Lukashev, E.; Zagidullin, V.; Pachenko, V.; Rakovich, Y. P.; Donegan, J. F.; Rubin, A. B.; Govorov, A. O. *Angew. Chem., Int. Ed.* **2010**, *49*, 7217−7221.
(7) Algar, W. R.; Tavares, A. J.; Krull, U. J. *Anal. Chim. Acta* **2010**, *673*, 1−25.
(8) Clapp, A. R.; Medintz, I. L.; Fisher, B. R.; Anderson, G. P.; Mattoussi, H. *J. Am. Chem. Soc.* **2005**, *127*, 1242−1250.
(9) Hildebrandt, N.; Charbonnière, L. J.; Beck, M.; Ziessel, R. F.; Löhmannsröben, H. G. *Angew. Chem., Int. Ed.* **2005**, *44*, 7612−7615.
(10) Charbonnière, L. J.; Hildebrandt, N.; Ziessel, R. F.; Löhmannsröben, H. G. *J. Am. Chem. Soc.* **2006**, *128*, 12800−12809.
(11) Geißler, D.; Charbonnière, L. J.; Ziessel, R. F.; Butlin, N. G.; Löhmannsröben, H. G.; Hildebrandt, N. *Angew. Chem., Int. Ed.* **2010**, *49*, 1396−1401.
(12) Morgner, F.; Geißler, D.; Stufler, S.; Butlin, N. G.; Löhmannsröben, H. G.; Hildebrandt, N. *Angew. Chem., Int. Ed.* **2010**, *49*, 7570−7574.
(13) So, M. K.; Xu, C. J.; Loening, A. M.; Gambhir, S. S.; Rao, J. H. *Nat. Biotechnol.* **2006**, *24*, 339−343.
(14) Xia, Z. Y.; Xing, Y.; So, M. K.; Koh, A. L.; Sinclair, R.; Rao, J. H. *Anal. Chem.* **2008**, *80*, 8649−8655.
(15) Liu, X.; Freeman, R.; Golub, E.; Willner, I. *ACS Nano* **2011**, *5*, 7648−7655.
(16) Freeman, R.; Liu, X. Q.; Willner, I. *J. Am. Chem. Soc.* **2011**, *133*, 11597−11604.
(17) Seker, U. O. S.; Ozel, T.; Demir, H. V. *Nano Lett.* **2011**, *11*, 1530−1539.
(18) Achermann, M.; Jong, S.; Balet, L.; Montano, G. A.; Hollingsworth, J. A. *ACS Nano* **2011**, *5*, 1761−1768.
(19) Feng, C. L.; Zhong, X. H.; Steinhart, M.; Caminade, A. M.; Majoral, J. P.; Knoll, W. *Small* **2008**, *4*, 566−571.
(20) Medintz, I. L.; Clapp, A. R.; Mattoussi, H.; Goldman, E. R.; Fisher, B.; Mauro, J. M. *Nat. Mater.* **2003**, 2.
(21) Geissbuehler, I.; Hovius, R.; Martinez, K. L.; Adrian, M.; Thampi, K. R.; Vogel, H. *Angew. Chem., Int. Ed.* **2005**, *44*, 1388−1392.
(22) Lu, H.; Schöps, O.; Woggon, U.; Niemeyer, C. M. *J. Am. Chem. Soc.* **2008**, *130*, 4815−4827.
(23) Boeneman, K.; Prasuhn, D. E.; Blanco-Canosa, J. B.; Dawson, P. E.; Melinger, J. S.; Ancona, M.; Stewart, M. H.; Susumu, K.; Huston, A.; Medintz, I. L. *J. Am. Chem. Soc.* **2010**, *132*, 18177−18190.
(24) Mei, B. C.; Susumu, K.; Medintz, I. L.; Delehanty, J. B.; Mountziaris, T. J.; Mattoussi, H. *J. Mater. Chem.* **2008**, *18*, 4949−4958.
(25) Mei, B. C.; Susumu, K.; Medintz, I. L.; Mattoussi, H. *Nat. Protocols* **2009**, *4*, 412−423.
(26) Schnolzer, M.; Alewood, P.; Jones, A.; Alewood, D.; Kent, S. B. H. *Int. J. Pept. Protein Res.* **1992**, *40*, 180−193.
(27) Prasuhn, D. E.; Feltz, A.; Blanco-Canosa, J. B.; Susumu, K.; Stewart, M. H.; Mei, B. C.; Yakovlev, A. V.; Loukou, C.; Mallet, J. M.; Oheim, M.; Dawson, P. E.; Medintz, I. L. *ACS Nano* **2010**, *4*, 5487−5497.
(28) Xu, J.; Corneillie, T. M.; Moore, E. G.; Law, G. L.; Butlin, N. G.; Raymond, K. N. *J. Am. Chem. Soc.* **2011**, *133*, 19900−19910.
(29) Medintz, I. L.; Berti, L.; Pons, T.; Grimes, A. F.; English, D. S.; Alessandrini, A.; Facci, P.; Mattoussi, H. *Nano Lett.* **2007**, *7*, 1741−1748.
(30) Dennis, A. M.; Sotto, D. C.; Mei, B. C.; Medintz, I. L.; Mattoussi, H.; Bao, G. *Bioconjugate Chem.* **2010**, *21*, 1160−1170.
(31) Sapsford, K. E.; Pons, T.; Medintz, I. L.; Higashiya, S.; Brunel, F. M.; Dawson, P. E.; Mattoussi, H. *J. Phys. Chem. C* **2007**, *111*, 11528−11538.
(32) Prasuhn, D. E.; Deschamps, J. R.; Susumu, K.; Stewart, M. H.; Boeneman, K.; Blanco-Canosa, J. B.; Dawson, P. E.; Medintz, I. L. *Small* **2010**, *6*, 555−564.
(33) Charbonnière, L. J.; Hildebrandt, N. *Eur. J. Inorg. Chem.* **2008**, *21*, 3241−3251.
(34) Boeneman, K.; Deschamps, J. R.; Buckhout-White, S.; Prasuhn, D. E.; Blanco-Canosa, J. B.; Dawson, P. E.; Stewart, M. H.; Susumu, K.; Goldman, E. R.; Ancona, M.; Medintz, I. L. *ACS Nano* **2010**, *4*, 7253−7266.
(35) Algar, W. R.; Krull, U. J. *Anal. Chim. Acta* **2007**, *581*, 193−201.
(36) Boeneman, K.; Mei, B. C.; Dennis, A. M.; Bao, G.; Deschamps, J. R.; Mattoussi, H.; Medintz, I. L. *J. Am. Chem. Soc.* **2009**, *131*, 3828−3829.
(37) Clapp, A. R.; Medintz, I. L.; Mauro, J. M.; Fisher, B. R.; Bawendi, M. G.; Mattoussi, H. *J. Am. Chem. Soc.* **2004**, *126*, 301−310.
(38) Medintz, I. L.; Clapp, A. R.; Brunel, F. M.; Tiefenbrunn, T.; Uyeda, H. T.; Chang, E. L.; Deschamps, J. R.; Dawson, P. E.; Mattoussi, H. *Nat. Mater.* **2006**, *5*, 581−589.
(39) Shi, Z. S.; Olson, C. A.; Bell, A. J.; Kallenbach, R. N. *Biopolymers* **2001**, *60*, 366−380.
(40) Sapsford, K. E.; Granek, J.; Deschamps, J. R.; Boeneman, K.; Blanco-Canosa, J. B.; Dawson, P. E.; Susumu, K.; Stewart, M. H.; Medintz, I. L. *ACS Nano* **2011**, *5*, 2687−2699.
(41) Sapsford, K. E.; Farrell, D.; Sun, S.; Rasooly, A.; Mattoussi, H.; Medintz, I. L. *Sens. Actuators, B* **2009**, *139*, 13−21.
(42) Zhou, D.; Ying, L.; Hong, X.; Hall, E. A.; Abell, C.; Klenerman, D. *Langmuir* **2008**, *24*, 1659−1664.
(43) Algar, W. R.; Krull, U. J. *Anal. Chem.* **2009**, *81*, 4113−4120.
(44) Algar, W. R.; Krull, U. J. *Anal. Bioanal. Chem.* **2010**, *398*, 2439−2449.
(45) Resch-Genger, U.; Grabolle, M.; Cavaliere-Jaricot, S.; Nitschke, R.; Nann, T. *Nat. Methods* **2008**, *5*, 763−775.

(46) Prasuhn, D. E.; Blanco-Canosa, J. B.; Vora, G. J.; Delehanty, J. B.; Susumu, K.; Mei, B. C.; Dawson, P. E.; Medintz, I. L. *ACS Nano* **2010**, *4*, 267−278.
(47) Delehanty, J. B.; Medintz, I. L.; Pons, T.; Brunel, F. M.; Dawson, P. E.; Mattoussi, H. *Bioconjugate Chem.* **2006**, *17*, 920−927.
(48) Medintz, I. L.; Pons, T.; Delehanty, J. B.; Susumu, K.; Brunel, F. M.; Dawson, P. E.; Mattoussi, H. *Bioconjugate Chem.* **2008**, *19*, 1785−1795.
(49) Akerman, M. E.; Chan, W. C. W.; Laakkonen, P.; Bhatia, S. N.; Ruoslahti, E. *Proc. Natl. Acad. Sci. U.S.A.* **2002**, *99*, 12617−12621.
(50) Derfus, A. M.; Chan, W. C. W.; Bhatia, S. N. *Adv. Mater.* **2004**, *16*, 961−966.
(51) Ruan, G.; Agrawal, A.; Marcus, A. I.; Nie, S. *J. Am. Chem. Soc.* **2007**, *129*, 14759−14766.
(52) Walker, B. J.; Bulovic, V.; Bawendi, M. G. *Nano Lett.* **2010**, *10*, 3995−3999.
(53) Pons, T.; Medintz, I. L.; Wang, X.; English, D. S.; Mattoussi, H. *J. Am. Chem. Soc.* **2006**, *128*, 15324−15331.
(54) Xiao, M.; Selvin, P. R. *J. Am. Chem. Soc.* **2001**, *123*, 7067−7073.
(55) Algar, W. R.; Krull, U. J. *Sensors* **2011**, *11*, 6214−6236.
(56) Bachmann, L.; Zezell, D. M.; Ribeiro, A. d. C.; Gomes, L.; Ito, A. S. *Appl. Spectrosc.* **2006**, *41*, 575−590.
(57) Elmore, S. *Toxicol. Pathol.* **2007**, *35*, 495−516.
(58) Liu, W.; Howarth, M.; Greytak, A. B.; Zheng, Y.; Nocera, D. G.; Ting, A. Y.; Bawendi, M. G. *J. Am. Chem. Soc.* **2008**, *130*, 1274−1284.
(59) Yu, W. W.; Chang, E.; Falkner, J. C.; Zhang, J.; Al-Somali, A. M.; Sayes, C. M.; Johns, J.; Drezek, R.; Colvin, V. L. *J. Am. Chem. Soc.* **2007**, *129*, 2871−2879.
(60) Clapp, A. R.; Medintz, I. L.; Uyeda, H. T.; Fisher, B. R.; Goldman, E. R.; Bawendi, M. G.; Mattoussi, H. *J. Am. Chem. Soc.* **2005**, *127*, 18212−18221.
(61) Zhang, C. Y.; Hu, J. *Anal. Chem.* **2010**, *82*, 1921−1927.
(62) Zhang, C. Y.; Yeh, H. C.; Kuroki, M. T.; Wang, T. H. *Nat. Mater.* **2005**, *4*, 826−831.
(63) Lim, T. C.; Bailey, V. J.; Ho, Y. P.; Wang, T. H. *Nanotechnology* **2008**, *19*, 075701.
(64) Kim, J. H.; Morikis, D.; Ozkan, M. *Sens. Actuators, B* **2004**, *102*, 315−319.
(65) Cady, N. C.; Strickland, A. D.; Batt, C. A. *Mol. Cell. Probes* **2007**, *21*, 116−124.
(66) Kim, Y. P.; Oh, Y. H.; Oh, E.; Ko, S.; Han, M. K.; Kim, H. S. *Anal. Chem.* **2008**, *80*, 4634−4641.
(67) Rodems, S. M.; Hamman, B. D.; Lin, C.; Zhao, J.; Shah, S.; Heidary, D.; Makings, L.; Stack, J. H.; Pollok, B. A. *Assay Drug Dev. Technol.* **2002**, *1*, 9−19.